Automated De-bonding and Peeling of Molded PDMS Layers for Microfluidic Device Production

A Dissertation
Presented to
The Academic Faculty

by

David Fender

In Partial Fulfillment
of the Requirements for the Degree
Master of Science in the
School of Mechanical Engineering

Georgia Institute of Technology
August 2019

Automated De-bonding and Peeling of Molded PDMS Layers for Microfluidic Device Production

Approved by:

Dr. Shreyes Melkote, Advisor
School of Mechanical Engineering
Georgia Institute of Technology

Dr. Stephen Balakirsky, Co-Advisor
Georgia Tech Research Institute
Georgia Institute of Technology

Dr. Christopher Saldana
School of Mechanical Engineering
Georgia Institute of Technology

Date Approved: August 12, 2019

ACKNOWLEDGEMENTS

I would like to thank my advisors; Dr. Shreyes Melkote and Dr. Stephen Balakirsky, for making my thesis possible, and for providing tremendous support throughout the process. Dr. Melkote assisted in many aspects of machining practices, which were a foundation of my research. Additionally, Dr. Melkote provided consistent technical guidance on effective research methodologies.

The progress made in robotic automation was only successful due to Dr. Balakirsky's expertise and commitment. Dr. Balakirsky, as well as Dr. LaVonda Brown assisted in the areas of robotics and coding, which was critical in understanding and developing the automation process. Our joint meetings shared knowledge from various backgrounds, which helped to collectively determine appropriate paths forward.

I am also grateful for the numerous pieces of equipment that were provided through Georgia Tech Research Institute (GTRI) and the Precision Machining Research Consortium (PMRC). Most notably, these include the computer numerical control (CNC) milling machine, as well as the Universal Robotics UR5 robot arm. GTRI also supplied many materials involved in metal mold making and custom equipment.

I was also assisted greatly in countless machining techniques by Vinh Nguyen, as well as the employees of the Montgomery Machining Mall. Finally, I would like to thank Dr. Wilbur Lam and Reginald Tran for sharing their knowledge and resources regarding microfluidic devices, and their assistance in automation efforts.

TABLE OF CONTENTS

LIST OF TABLES

LIST OF FIGURES

SUMMARY

Polydimethylsiloxane (PDMS) based microfluidic devices contain micro-scale channels, which are used for routing fluids in bio-chemical analysis. The existing methods for producing such microfluidic devices are highly labor intensive and require expensive materials (e.g. silicon wafer) and processes (e.g. photolithography). An alternative approach is to use a machined metal mold for curing the PDMS layers, which are then assembled into a device. Aluminum molds allow for greater durability and longevity compared to silicon wafers.

Robotic automation can further reduce cost and increase productivity; however, no known existing methods for automation of microfluidic devices are available. This thesis investigates innovative methods for automating the process of creating and assembling the PDMS layers used to produce microfluidic devices. Robotics can be used to automate many of the steps involved in making the devices, including curing the PDMS polymer. However, the process of removing the PDMS from the mold currently involves human manipulation. This requires innovative methods to be developed in order to enable robotic automation of PDMS microfluidic device layer removal from a metal mold.

To allow for successful robotic removal of the PDMS device layer from the mold, the adhesion between the PDMS and metal mold must be de-bonded, followed by a peeling operation. This thesis discusses the experimental evaluation of different methods for robotic de-bonding and peeling of cured PDMS layers from a machined aluminum mold.

Successful automation equipment should be cost effective to produce, involving reusable equipment or low-cost disposable supplies. Testing involved 3D printed parts for

prototyping. Initial methods utilized mechanical devices to lift and remove the PDMS from the mold. Continuous refinements progressed toward a two-step method of de-bonding with pressurized air from a needle, followed by peeling with a suction cup. Controlling the air pressure and manipulating the suction cup required systematic testing and force analysis. This thesis details the characteristics associated with PDMS removal, and the specific techniques required for reliable automation.

INTRODUCTION

1.1 Background

Microfluidics is the study of controlling and manipulating the flow of fluids through a network of micro-scale channels contained in a device designed for bio-chemical analysis. These micro-scale channels allow for optimized utilization of expensive medicines during research and development. This is due to the increased surface area to volume ratio as the dimensions are reduced. Therefore, an increased rate of interaction will occur between the medicines and the cells they are intended to treat [1]. Microfluidic devices can be made with plastics, glass, and elastomers. One common method of creating microfluidic devices is the use of a molded silicone polymer, such as Polydimethylsiloxane (PDMS). PDMS is used due to its optical clarity, ease of molding, and its chemical stability. Microfluidic devices are usually made using molds produced by photolithography on a silicon wafer. This process involves coating a wafer with a photoresist, such as MicroChem SU-8, and using a mask to create the desired channels. PDMS is then spin-coated on the silicon wafer with channels. The final steps are to cure the PDMS, remove from the mold, and lastly bond to a glass or PDMS substrate to enclose the channels. Alternatively, microfluidic devices can be molded and cured using a hot embossing method, pressing a heated master mold onto partially cured PDMS, until curing is complete. Figure 1 below shows the current process of producing the mold and microfluidic device.

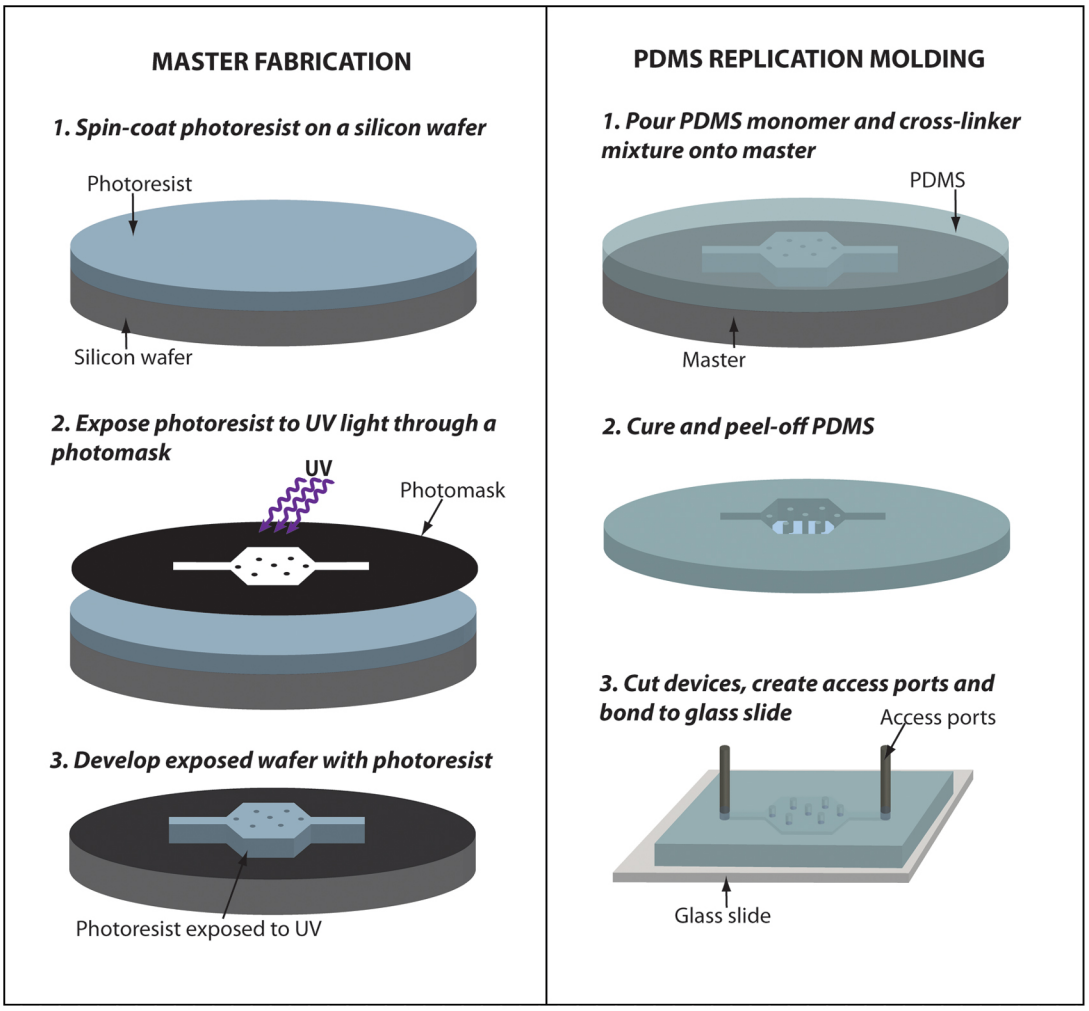

Figure 1 - Current production process of mold and microfluidic devices [26]

The current process of producing microfluidic devices is an entirely manual process, involving many steps, as well as expensive materials. One method of reducing the cost is to create the mold out of machined metal, rather than by photolithography. The metal mold is much cheaper to produce, does not require a clean room environment, and allows for virtually unlimited molding replications of PDMS. In contrast, the photoresist channels can only be used for molding and curing PDMS 25-50 times, before beginning to break down, and require a new silicon wafer with repeated photolithography. Metal molds also allow

for higher curing temperatures, which reduces the time required. The SU-8 photoresist is only capable of withstanding temperatures up to 80 degrees Celsius. At that temperature, PDMS requires 30 minutes to fully cure. In contrast, PDMS can be cured in only 10 minutes at 120°C, a temperature very obtainable with a metal mold.

The use of a metal mold reduces more than half of the overall steps involved in producing microfluidic devices, given that the photolithography process is more involved. This method, with reduced steps and greater mold longevity, makes it practical to perform robotic automation of the entire production process. While the process may appear to be suitable for automation, there has been no published research on the specific tasks and/or equipment required to enable robots to substitute human manipulation in microfluidic device production.

1.2 Motivation

The field of microfluidics is continuously growing, as biomedical research and knowledge expands. However, production of microfluidic devices remains a tedious and time-consuming process. This requires graduate students, scientists and engineers to dedicate a portion of their time performing these repetitive tasks, rather than on their intended research.

Robotic automation of microfluidic device production would allow for lower material costs, and greatly reduced labor costs. With the reduced cost of entry-level robotics, and recent advancements in control techniques, it is feasible to create an automated system for the production of microfluidic devices for corporate and university research laboratories. With this objective in mind, the processes must be compact,

simplistic, flexible, and highly reliable. Additionally, affordable robots and flexible equipment is required to make the system practical for the application and end user.

While the use of microfluidic devices allows for reduced research and development costs of bio-medical testing, the expenses and time commitment of device production can hinder progress [3]. A fully automated process for producing microfluidic devices would reduce the costs to only the initial price of a machined open mold, and the relatively small cost of PDMS polymer per device.

1.3 Research Objective

The objective of this thesis is to study the feasibility of automating a key step in the PDMS-based microfluidic device production process utilizing a machined metal mold. Specifically, the process of de-bonding and removing (via peeling) the cured PDMS layer from the metal mold is a challenging task due to the presence of adhesive bonding forces between the PDMS and the mold. In order to achieve these goals, innovative mold-making, and automated PDMS layer removal methods are required and form the central focus of this thesis.

The specific research objectives of this thesis are the following:

1. Develop a machining process to produce a suitable metal mold for microfluidic device
2. Develop and evaluate methods for automated removal of a cured PDMS layer from the metal mold

1.4 Approach

The main research objective of this thesis is to develop an effective approach for producing the PDMS layers used to construct a stackable microfluidic device. However, first a metal mold with properties applicable for microfluidic devices must be produced. The initial approach is to utilize a mechanical machining process such as milling to create a metallic (aluminum) mold. This involves identifying suitable machining conditions to produce an aluminum mold of suitable quality. The next step involves developing the procedures to mold the PDMS in the metal mold. As part of this step, important characteristics of PDMS including its adhesion to the mold, as well as elasticity and durability are analyzed. These factors play critical roles in the approach used to remove the PDMS from the mold. Various low-cost and simple methods for robot-aided removal of the molded PDMS layers are then proposed and experimentally evaluated to determine their advantages and drawbacks in order to identify the ideal approach for mass automation.

1.5 Thesis Outline

The structure of the thesis is as follows. Chapter 2 details prior research and relevant knowledge in the field of general adhesion and peeling, as well as in microfluidic device production. This provides for a strong fundamental understanding of the current processes, and for a potential solution for robotic automation. Chapter 3 discusses the machining (milling) of aluminum molds, and the resulting mold characteristics as a function of the machining parameters. Chapter 4 introduces initial methods for peeling the cured PDMS from the molds, including findings associated with each method. Chapter 5 presents the results of refined methods for removing cured PDMS from the mold. Specifically, this

includes a two-step removal process of de-bonding the PDMS from the metal mold, following by a robot-aided peeling process. Chapter 6 concludes the thesis, discussing primary findings for a path forward in microfluidic device production. Lastly, Chapter 7 discusses future developments and recommendations, specifically in the area of robotic optimization to allow for a broad user base.

CHAPTER 2. LITERATURE REVIEW

2.1 Introduction

This chapter discusses existing literature in microfluidics, specifically in the areas of mold machining, and characteristics of de-bonding and peeling PDMS. There is considerable existing knowledge in the area of machining methods for producing microfluidic device molds. This encompasses the processes of creating the molds, as well as steps for curing PDMS in the machined molds. Due to the entirely manual production process for microfluidic devices, there is no published research on specific PDMS removal methods. However, there is literature discussing the general peeling properties of PDMS and other adhesive materials. This knowledge can be used to guide the research approach for automated removal of PDMS from the mold.

2.2 Polymer-based Microfluidic Device Fabrication

Microfluidic devices can be fabricated using a variety of materials, including glass, plastics, and silicone polymers [2]. Over the past decade, PDMS has become the standard material used in microfluidic device production, due to the ease of molding and bonding. There are numerous methods of creating the channels in microfluidic devices, from hot embossing to injection molding [3]. Hot embossing is one of the most common methods, involving pressing a heated silicon mold with protruding channels into a plastic, such as Polymethyl methacrylate (PMMA) to melt the desired channels into the material. Similarly, soft lithography is the same process, but instead is used to cure “soft” elastomeric materials, such as PDMS. Both methods involve creating protrusions on a silicon wafer to mold the

channels in the device. These channels are created by coating the wafer in a photoresist material, which cures under ultraviolet (UV) light. The shape of the channels is produced by covering the wafer with a photomask, that only allows light to pass through in the desired locations. This cures the channel protrusions to be used for molding the polymer. The remaining uncured photoresist is rinsed away to create the final mold. The benefits of photolithography on a silicon wafer include the ability to produce channels with accurate dimension and a smooth surface finish. Additionally, photolithography allows for ease of prototyping and low cost for short runs. In comparison, injection molding typically costs $20,000 to $30,000 for one mold [2].

2.3 Machined Metal Molds

Creating microfluidic devices with machined metal molds has become a more common method due to the reduction in time, cost, and equipment required [11]. Metal blocks are machined as a positive master mold, recessed in a pocket, into which the uncured PDMS is poured. Similarly, metal or plastic blocks can be machined and pressed/stamped into partially cured PDMS until curing is complete. For both methods, positive protrusions in the mold create the channels in the PDMS. The PDMS layer is then bonded to a substrate of glass or PDMS to enclose these channels. Figure 2 illustrates machining of the positive mold and pressing into partially cured PDMS.

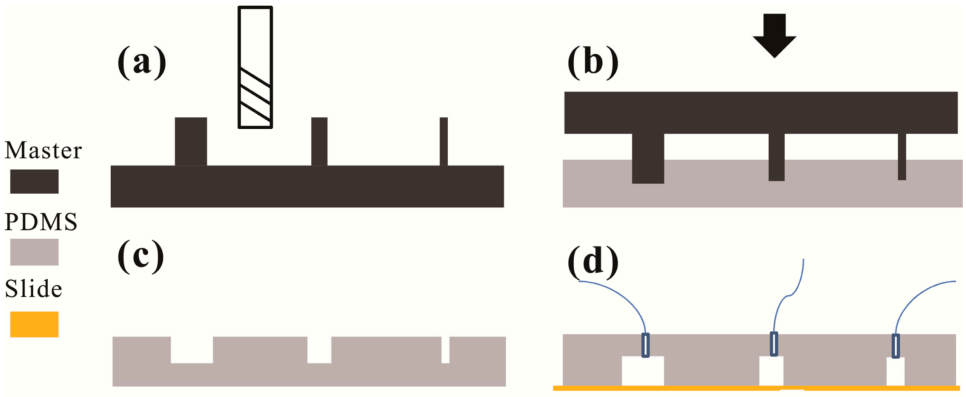

Figure 2 - Machining of microfluidic master mold for fabricating microfluidic device. (a) positive master mold is milled; (b) mold is pressed into partially cured PDMS; (c) cured PDMS is separated from mold; (d) PDMS layer is bonded to glass substrate to enclose channels [11]

This article demonstrates the ability for molding PDMS with a machined (milled) mold, replacing the use of photolithography [11]. For machined molds to substitute silicon molds, ideal conditions for surface roughness and tolerance must be met. There is existing literature on the effects of machining parameters on surface roughness for general cutting. Additionally, existing literature details the effects that surface roughness has on the adhesion and bond strength between PDMS and metal molds. As a benchmark, silicon molds have a very smooth surface in the range of 0.1 to 0.4 nm Sq. [17]. A smooth molding surface for microfluidic devices is important for promoting optical clarity and improving bond strength [14]. While it is not reasonable to expect the same surface finish as a polished silicon mold in a machined metal mold, it is desirable to obtain similar properties.

A study was performed by Yousuff, et al., on the optimal cutting parameters of a micro milling process used to produce an aluminum mold for microfluidic devices [12]. The study measured the effects of the micro milling parameters on both surface roughness and bond strength between the molded PDMS and various substrates. Micro end mills of diameter 200 μm and 400 μm were tested, with spindle speeds of 10,000 to 20,000 rpm,

and feed rates of 50 to 150 mm/min. Axial depths of cut of 5, 10, and 15 μm were also evaluated. The study found that the feed rate had the greatest impact on surface roughness, and the depth of cut had the least impact [12]. The specific cutting parameters tested that resulted in the smoothest finish with the 200 μm diameter end mill was the following: 20,000 rpm spindle speed, 50 mm/min feed rate, 5 μm depth of cut. These results show that a higher spindle speed, slower feed rate, and smaller depths of cut will result in the lowest values of surface roughness. With these parameters, the lowest arithmetic average surface roughness (Ra) was 0.169 μm. Conversely, the opposite cutting conditions with lower spindle speed, faster feed rate, and larger depth of cut, with the 400 μm diameter tool resulted in a surface roughness of up to 0.389 μm. The results also showed that the 200 μm diameter tool yielded 30-40 percent lower surface roughness than the 400 μm diameter tool. This can be attributed to the larger diameter tool removing more material, resulting in larger burrs [12].

One of the main effects of surface roughness is on the bond strength of PDMS with different substrates [12]. With a smoother surface, there is greater contact area between the bonding surfaces. This relationship between mold surface roughness and bond strength between PDMS and different substrates is shown in Table 1.

Table 1 - Effects of surface roughness on bond strength [12]

Surface Roughness (μm)	Bonding Strength (kPa)				
	Oxygen Plasma Treatment		UV-Ozone Treatment		PDMS Adhesive and Partially Cured PDMS
	PDMS–Glass	PDMS–PDMS	PDMS–Glass	PDMS–PDMS	PDMS–PDMS and PDMS–Glass
0.17	270 ± 20	180 ± 20	314 ± 20	95 ± 20	>500 kPa
0.27	263 ± 20	168 ± 20	301 ± 20	92 ± 20	>500 kPa
0.32	228 ± 20	147 ± 20	288 ± 20	92 ± 20	>500 kPa
0.4	185 ± 20	105 ± 30	270 ± 20	87 ± 20	>500 kPa

The table presents three different methods of bonding PDMS layers, including plasma treatment, UV-ozone, compared to partially cured PDMS as an adhesive layer (which is then cured). For plasma treatment, there is a 30 to 40 percent reduction in bond strength when the surface roughness increases from 0.17 to 0.4 μm. Given that microfluidic devices route fluids between the molded PDMS layer and the substrate, a strong bond is critical for ensuring leakage does not occur.

Additional work has been published using metal molds for hot embossing PDMS and PMMA for rapid fabrication of microfluidic devices, using readily available equipment [5]. These publications, however, do not go into depth regarding the ideal machining parameters and the effects on surface roughness. Instead, they adopt a slower feed rate and higher spindle speed within the capabilities of the machine tool used.

2.4 Adhesives and Peeling

2.4.1 *Speed and Adhesive Energy*

While previous attempts on automated peeling of microfluidic devices has not been reported, existing literature can offer insight into potential methods. Transfer printing involves transporting inks or miniature structures between substrates. One method of performing this is by controlling the kinetic energy to adjust the levels of adhesion[19]. Structures can be transported using a rate sensitive elastomer, such as PDMS. By increasing the velocity of an elastomer, the adhesive energy increases [20]. In the application of transfer printing, an elastomeric stamp is placed on a structure that is to be transported. The stamp is then retracted at a high velocity, which provides for an increase in adhesion between the stamp, and the object. This overcomes the adhesive and gravitational forces

between the object and the substrate it was resting on, which allows it to be lifted. The structure is then placed at the desired location, where the stamp is then retracted slowly. This slow retraction has a lower level of adhesion between the stamp and object, allowing the structure to be released. Figure 3 shows the steps of transfer printing with an elastomeric stamp.

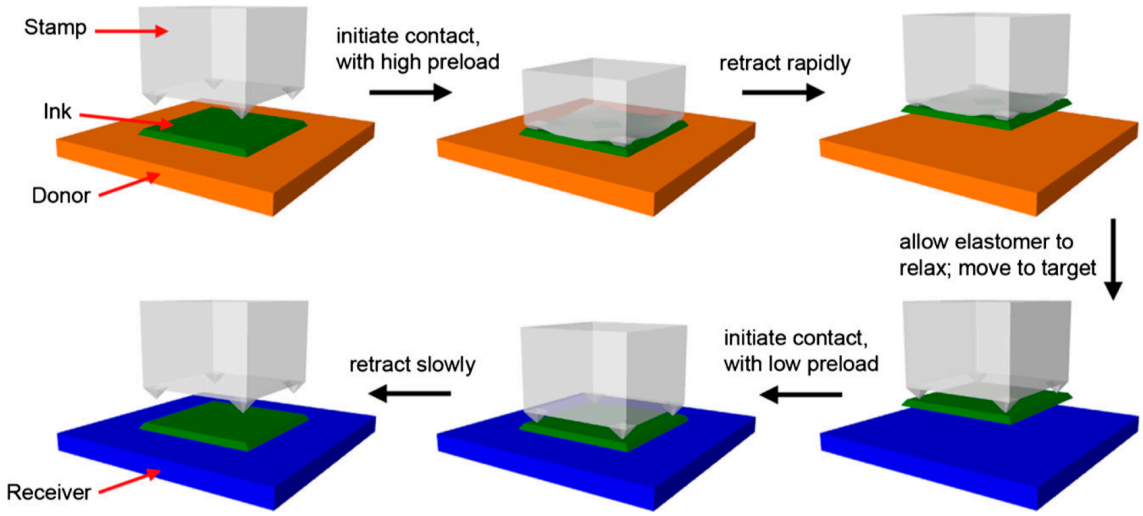

Figure 3 - Steps of transfer printing with an elastomeric stamp [19]

This relationship was determined mathematically by rolling a steel cylinder down a wedge-shaped elastomer. As acceleration due to gravity acts on the cylinder, the adhesive energy increases. Figure 4 shows a plot of the energy release rate based on the separation speed.

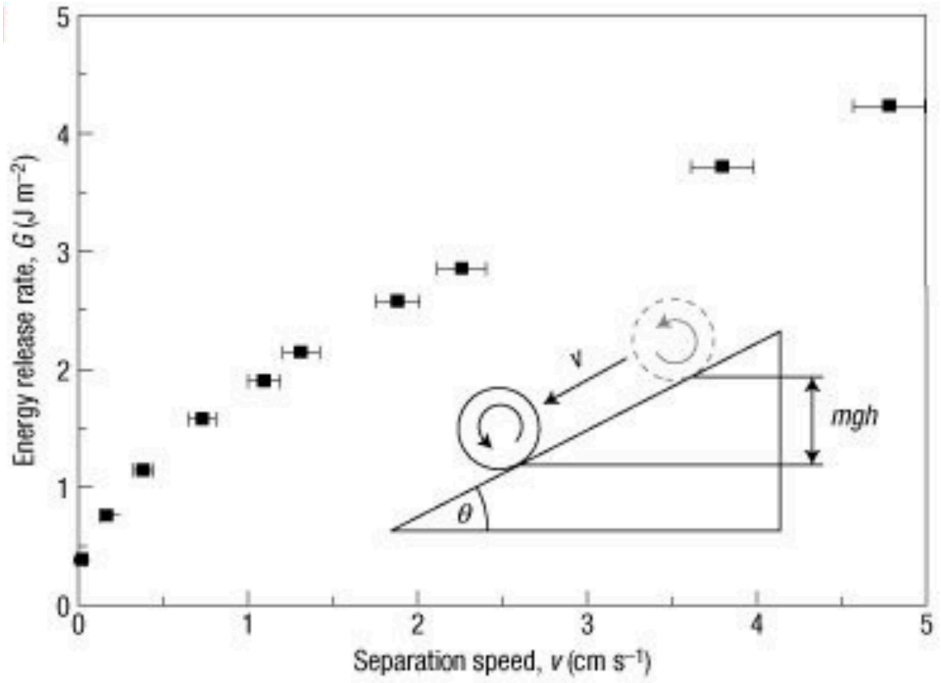

Figure 4 - Effect of separation speed on energy release rate [19]

The principle discussed here provides guidance when automating the peeling of PDMS based microfluidic devices from their mold. Therefore, to assist in peeling PDMS from a metal mold, slower separation speeds are preferred.

2.4.2 *Peel Angle*

In addition to separation (or peeling) speed, the peel angle is a factor that should be investigated to optimize the automation process. A low peeling force is again desirable to minimize potential damage to the PDMS layer. A test was performed where PDMS squares sized at 0.06” x 0.06” x 0.01” were peeled from a PMMA substrate, with varying peel angles [29]. Figure 5 illustrates the experimental setup used for peeling.

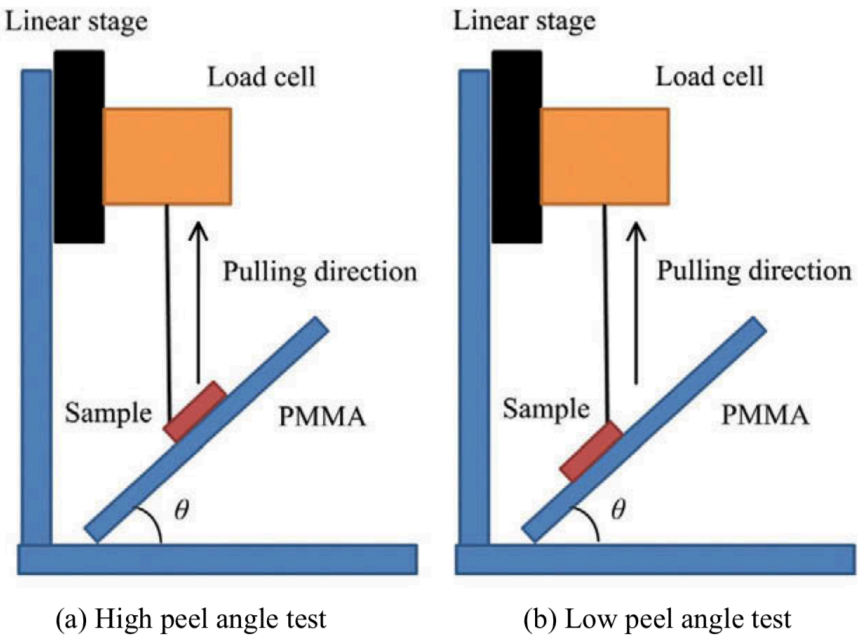

(a) High peel angle test (b) Low peel angle test

Figure 5 - Illustration of setup for testing peeling forces as varying angles [29]

Several peel angles were tested, including the angles represented in the figure above, namely 30 and 150 degrees, relative to the surface from which the PDMS is peeled. It was found that peel angles less than 90 degrees resulted in higher forces than when the angle was greater than 90 degrees. One test at a peel angle of 30 degrees and a speed of 1 mm/s resulted in a force per edge of approximately 350 mN/mm, compared to only about 10 mN/mm at a 150-degree peel angle [29]. This considerable decrease in peeling force can be attributed to the surface area of the adhesive that is under load during peeling [22]. Specifically, at lower peel angles, the elasticity of the material extends the peeling force inward toward a greater portion of the film. This in turn increases the adhesive energy. Conversely, a high peel angle applies force to only a thin area along the leading edge of the peel, which can greatly reduce the peeling force as discussed above.

2.5 Bond Strength

For PDMS to successfully be peeled from the mold, an understanding of the adhesive bond strength between the cured PDMS and various substrates must be obtained. Bond strength, measured in terms of the force per unit area of adhesion, provides guidance on potential removal methods, as well as concepts that can be eliminated. Tests were conducted to test the bond strength of PDMS on various substrates [25]. Bond strength was measured by inserting an air tube into bonded PDMS samples and subjecting them to increasing pressure until the bond strength was exceeded. Figure 6 shows the experimental setup with PDMS sample and the pressurized air source.

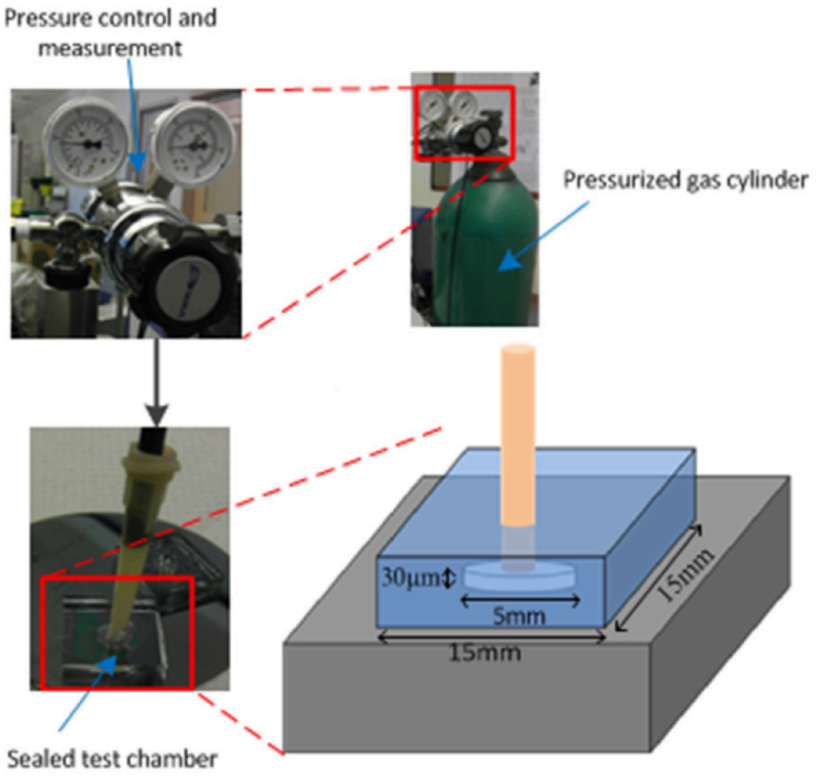

Figure 6 - Experimental setup testing bond strength using pressurized air [25]

The study found that PDMS bonded to silicone has a strength of 340 kPa, while PDMS bonded to aluminum has a strength of 269 kPa for a PDMS to cross-linker ratio of 10:1, which is typically used in microfluidics. After de-bonding, the adhesive forces are greatly reduced, to only the natural self-adhesion of PDMS. This adhesive strength is only 35 to 50 kPa. This reduction of bond strength will allow for improved workability of the PDMS to be removed from the mold. This study provides both knowledge of the bond strength, as well as an approach to de-bonding the PDMS.

2.6 Summary

Existing literature provides general guidance for machining metal molds, with lower feed rates and higher spindle speeds creating a low surface roughness for microfluidic devices. While specific automation methods are not publicly known, characteristics of PDMS, including adhesive properties are detailed. These characteristics include that the adhesion of elastomers increase with increasing rate of peel/retraction [19]. Additionally, increasing the peel angle between PDMS and the substrate it is being peeled from, decreases the force required [29]. Previous studies to measure the bond strength of PDMS to various substrates used pressurized air from a tube to expel air between the PDMS and the mold [25]. The existing literature assists in determining methods and processes that are suitable for automation.

CHAPTER 3. MOLD MACHINING

3.1 Machining Parameters

Before progress can be made on the automation aspect of the research, a metal mold, made of 6061 aluminum, must first be created. The literature search on mold machining provided limited guidance, specifically of the tools used, as they were restricted to very small diameter end mills. This requires that first the proper machining conditions must be determined. In order to best match the existing silicon wafer photolithography methods, a low surface roughness and tight tolerancing must be achieved. Molds for microfluidic devices are the positive master of the PDMS device. Therefore, making the channels of the microfluidic device require protrusions in the mold. Machining of these molds can be accomplished by using flat end mills to machine away the surrounding material to create the raised channels. The initial critical aspect to consider when machining is the diameter of the end mills used. Given that the channels are protruding, the spacing between the channels must be at least the diameter of the end mill. Therefore, if the channels are desired to be placed very close together, small diameter tools must be used to accomplish this.

The microfluidic mold to be replicated is in use by Dr. Wilbur Lam's laboratory of biomedical researchers at Georgia Tech, used for testing the effects of viruses on cells. This mold has channels of 4.5mm width, 100μm height, and 3mm channel spacing.

3.1.1 *Cutting Tools and Cutting Parameters*

The primary requirements for machining the aluminum mold include the tool used, the rotation speed of the spindle, and the feed rate of the workpiece. Important specifics of the tool are the diameter, material, and number of cutting teeth (flutes). The diameter of the tool affects the peripheral cutting speed of milling measured in m/min. Smaller tool diameters, such as those used in micro-milling will lower the cutting speed. To combat this, the spindle speed must increase, which is governed by the limits of the milling machine utilized. The CNC milling machine used for machining the mold was an Okuma MILLAC 44V, which has a maximum spindle speed of 12,000 rpm. Feed rate and flute number also have an impact on the final surface roughness. Both parameters affect the distance that the tool travels per tooth. The tool style chosen for machining are four flute carbide end mills.

The recommended cutting speed for machining aluminum with carbide end mills is 240 to 610 m/min [16]. However, in order to replicate Dr. Lam's mold, an end mill diameter of 1.588 mm (1/16") is required. With the maximum spindle speed of 12,000 rpm, a maximum cutting speed of only 60 m/min can be achieved. While this does not fall in the ideal range, slower feed speeds can be used to achieve a smoother surface finish. A baseline feed rate of 127 mm/min is used, as it is slow, yet still capable of machining a part in reasonable amount of time. A feed rate of 610 mm/min is also used, based on the recommended feed per tooth of 0.0127 mm [16].

3.2 Surface Roughness

A test was performed with the intent of comparing the resulting surface roughness obtained as a function of the feed rate, depth of cut, and tool path overlap. As discussed, feeds of 5 and 24 in/min will be used. Microfluidic devices have varying requirements for channel dimensions, so machining depths of 100µm and 200µm will be compared. Lastly, tool overlaps of the default 3 percent and an overlap of 30 percent will be used. In order to best replicate the machining process of a microfluidic device, sections of Dr. Lam's mold will be replicated with the combinations of each variable. Figure 7 below is an image of the test mold produced using the aforementioned cutting parameters.

Figure 7 – CNC milled aluminum mold with various machining parameters

A Zygo Zegage Optical Profiler was used to characterize the surface roughness of the machined aluminum mold. The Zygo works by adjusting the focus through a set distance range across an 828μm square viewing area. As each part of the surface goes into and out of focus, the MX MicroLite program calculates the surface based on the height profile.

3.2.1 *Results*

After machining the test sites on a block of aluminum, the surface roughness was measured in four (4) different locations using the Zygo. The surface roughness is measured as the root mean squared (RMS), denoted as Sq., across the viewing area. The results are shown in Table 2 below.

Table 2 - Effects of machining conditions on surface roughness RMS

	Sample 1 (μm)	Sample 2 (μm)	Sample 3 (μm)	Sample 4 (μm)	Average (μm)
100μm 127 mm/min 3% Overlap	0.112	0.112	0.206	0.206	0.159
100μm 610 mm/min 3% Overlap	0.263	0.273	0.333	0.312	0.295
200μm 127 mm/min 3% Overlap	0.110	0.088	0.396	0.394	0.247
200μm 610 mm/min 3 % Overlap	0.293	0.290	1.226	1.250	0.765
200μm 127 mm/min 30% Overlap	0.148	0.138	0.317	0.301	0.226
200μm 610 mm/min 30% Overlap	0.265	0.288	0.269	0.262	0.271

The results show that, the greatest factor in reducing surface roughness is the feed rate. Slow feed rates allow for minimizing tool deflection, which is shown to be notable for a tool of 1.588 mm (1/16”) diameter. When deflection is present at higher feed rates, however, surface roughness can be considerably reduced by increasing the percentage of tool path overlap. The tool deflects in the opposite direction of the feed, due to the force acting on the front of the tool during cutting. The curvature of the tool is then pressed deeper into the material, causing slight grooves. By increasing tool overlap, the width of these grooves is thinner, which decreases the overall variation in height. It should be noted that while the overall surface roughness can be reduced with increasing tool path overlap, the machining tolerance and/or offset will be altered due to the tool deflection. Tolerance will be discussed in the following section.

The desired surface roughness has yet to be determined though biomedical research. Generally, bonding to glass/PDMS to enclose the channels is stronger and more reliable with a smoother molded PDMS surface [12]. Until a specific range of surface roughness is determined for biomedical applications, machining at a feed rate of 127 mm/min is deemed adequate for progressing toward automation of the PDMS-based microfluidic device production process.

3.3 Tolerance

Microfluidic devices can be machined using a 2D milling operation, since they have vertical wall channels. While the machining pattern relies on the accuracy of the milling machine, human input is required to align the part. Microfluidic devices have a relatively large bezel surrounding the channels, of about 10 mm. The purpose of the bezel is to allow for trimming following manual removal of the PDMS layer, and also to increase area for

bonding to glass or PDMS to create the device. This bezel means that tight tolerances are not as critical in the X and Y directions. However, given that microfluidic channels can typically range in channel depths from about 25 to 200 microns, accurate setting of the Z-offset is required. While typical machining tolerances are about 25µm (0.001”), that would cause significant variation in channel depth. Therefore, a highly accurate method of setting the origin is required. One of the preferred methods is using a gage offset with dial indicator, which allows for quick and repeatable zeroing.

The Zygo was also used to measure the depth of cut of the channels. Figure 8 and Figure 9 below shows the machined surfaces under the microscope. The channels were first machined by face milling the pocket with a 25.4 mm (1”) end mill, then machining between the positive mold channels with the 1.588mm (1/16”) end mill.

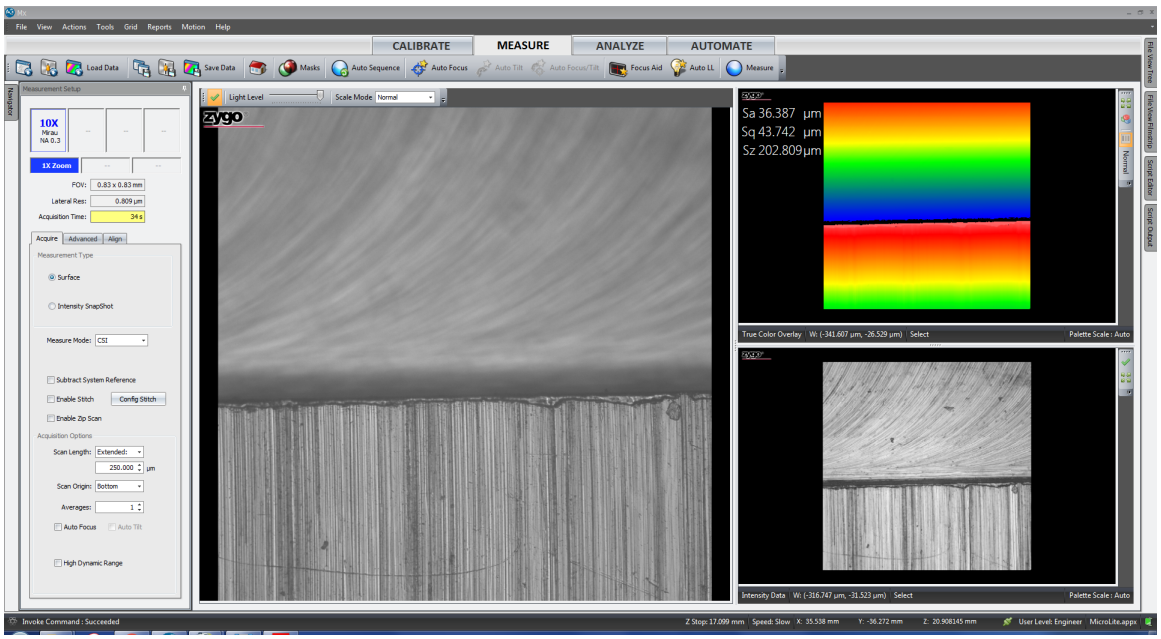

Figure 8 - MX Microlite program with microscopic view of face milled surface

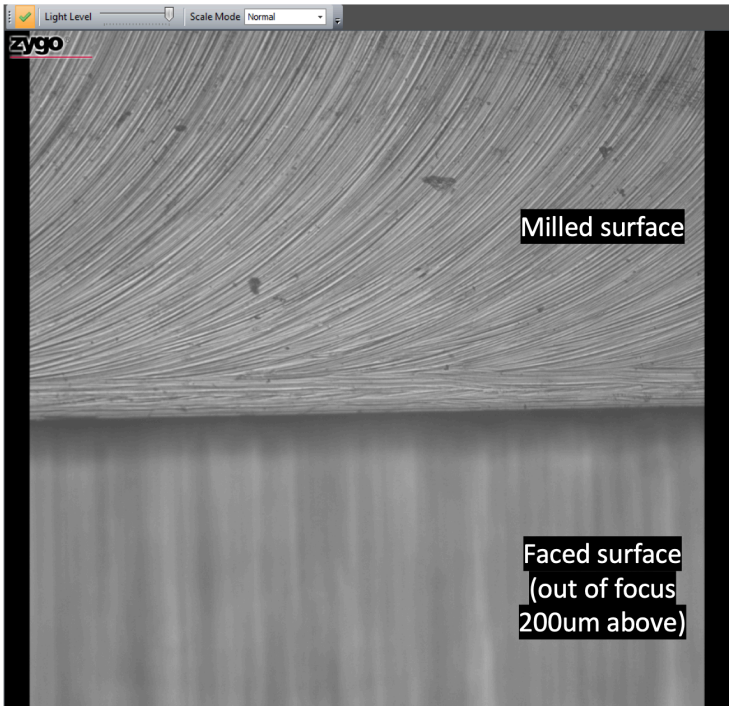

Figure 9 - Microscopic view of milled surface with 1.588mm (1/16") end mill

In order to obtain a measurement of the depth of cut in various locations, a line segment, or slice, is drawn in the MX program, following the scanning operation. This allows for variation in the depth to be determined. Figure 10 below shows the surface map and line slice.

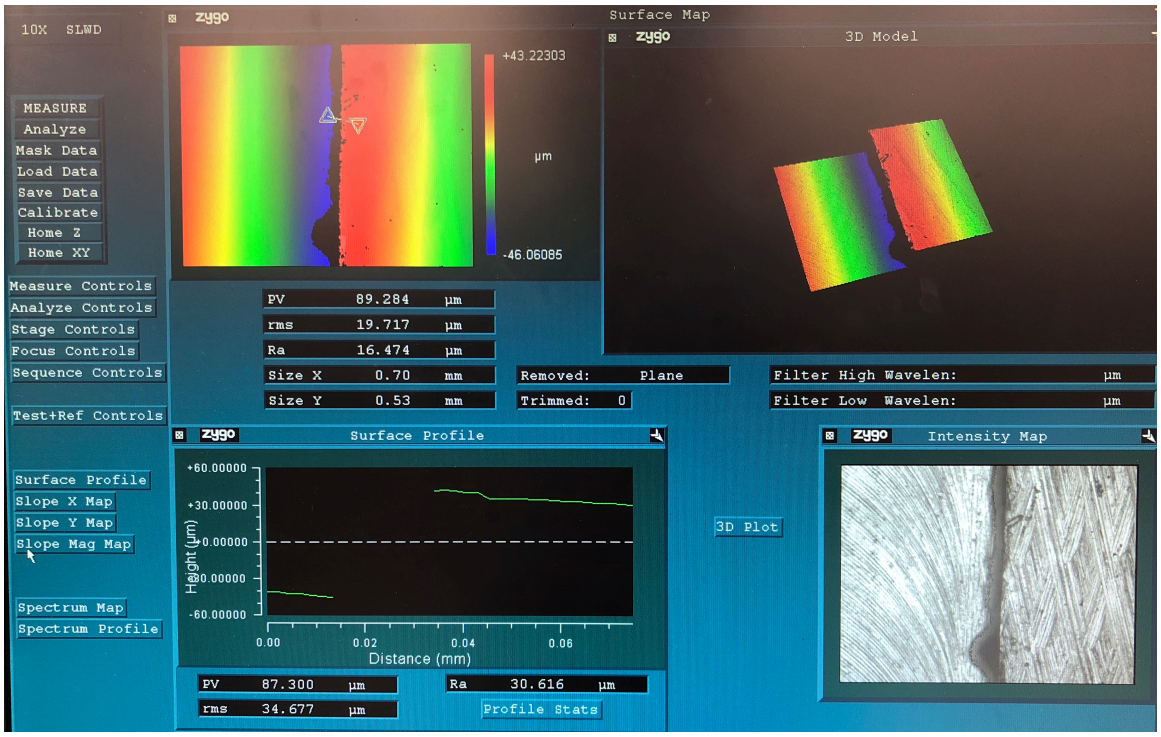

Figure 10 - MX surface profile map and depth of cut measurement

3.3.1 *Results*

A 120µm scan was performed in ten locations in the channels machined at 100µm, 127 mm/min, and 3 percent overlap. In each scan, five slices were recorded. Table 3 below shows the average of the five slices for each location, as well as the overall average and standard deviation.

Table 3 - Depth of cut measurements

	5 Sample Average (μm)
Location 1	96.88
Location 2	92.30
Location 3	94.14
Location 4	91.52
Location 5	92.42
Location 6	93.24
Location 7	93.98
Location 8	90.64
Location 9	88.80
Location 10	87.74
Overall Average	91.76
Standard Deviation	3.24

Although the average depth of cut was 8μm less than the target depth of 100μm, this can be adjusted for when setting the offset. A depth of cut smaller than intended can be caused by the upward force on the tool while machining. Using the gage offset with 2.5μm (0.0001”) accuracy, the offset can be adjusted accordingly for the desired post-machining depth. Improved accuracy can be obtained by ensuring a high-quality initial face milling operation of the part prior to setting the offsets for machining the pocket and channels. Given the high level of precision required, variation in the offset may occur during tool change operations. If this is determined to be significant, setting the offset and machining with each tool individually may be required. Additionally, alternative mold materials, such as stainless steel, will respond differently to cutting conditions. In order to obtain high precision results with a tolerance of approximately 2.5μm (0.0001”) or less,

calculating the correct offset may be required for each particular machine, tool, mold material, and possibly during each tool change operation. This is especially true if machining channels with shallower depths.

3.4 Microfluidic Mold Replication

Using the results obtained from the machining parameters above, the desired microfluidic device was machined. Additionally, these machining parameters will be used for various test molds for progress towards full automation of the microfluidic device production, as discussed in the following chapters. Figure 11 below shows the machined microfluidic device mold.

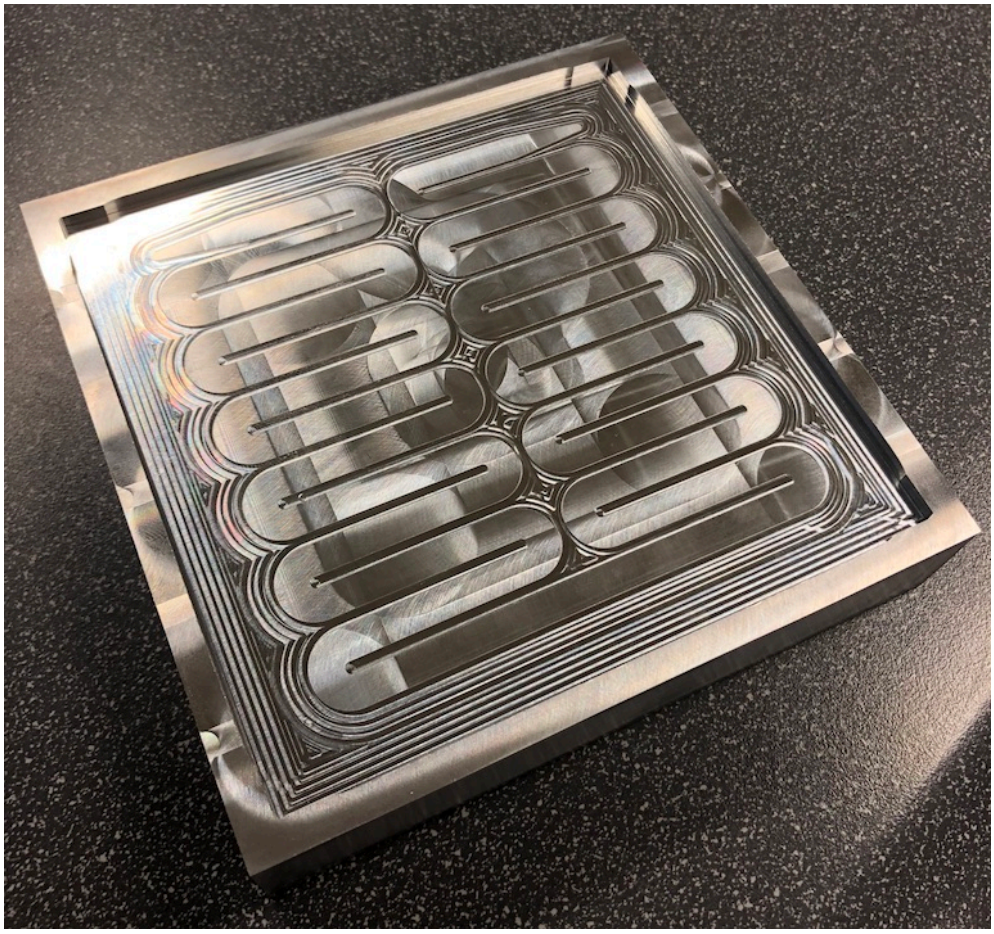

Figure 11 - CNC milled microfluidic device mold

3.5 Summary

In order to fabricate a PDMS microfluidic device, a mold was created using a CNC milled aluminum block. A suitable mold for microfluidic device must have a low surface roughness and tight tolerancing, given the micro-sized features of the device channels. Through experimentation, it was found that a slow feed rate of 127 mm/min, with a high spindle speed of 12,000 rpm, and a shallow depth of cut of 100 μm provided for a surface finish of about 0.150 μm Sq. (Table 2).

The tolerance associated with the channel depth can be accurate to within a few microns of the target depth. Setting a high accuracy of tool offset can be quickly and reliably achieved using a gauge offset with dial indicator.

CHAPTER 4. PEELING PDMS

4.1 Introduction

After machining the metal mold, the objective is to fully automate the process of microfluidic device production. This includes all steps from initial preparation of the liquid polymer, to final device assembly. In order to understand the potential challenges of automation, each step must be analyzed. Below is a list of the seven main tasks involved in producing the devices in a metal mold.

1) Mix polymer and crosslinker to produce PDMS
2) De-gas PDMS to remove air bubbles produced during mixing
3) Pour PDMS into mold
4) Cure PDMS in oven
5) Remove PDMS layer from mold
6) Punch holes for inlet/outlet tubing
7) Bond PDMS to glass/PDMS to enclose channels

Most of these steps involve relatively simple tasks for a robot to perform, such as a mixing operation, or placing a mold in an oven. However, the process of removing the cured PDMS from the mold will require an alternative approach than the current manual method. The manual method involves cutting around the perimeter of the PDMS device with a scalpel, trimming away a small amount of PDMS. The scalpel is then used to lift an edge of the PDMS, to enable peeling by hand. This process involves human manipulation and would be very difficult to reliably automate. Instead, a new approach must be created; one that utilizes practical equipment and involves simple and reliable operations.

4.2 Peeling Characteristics

In order to determine methods of removing the PDMS from the mold, an understanding of the material properties must be determined. PDMS has elastic and adhesive properties, but is also fragile and prone to tearing. Before testing specific robotic methods of removing the cured PDMS layer from the mold, experimentation of basic peeling characteristics will be gathered.

The measurands of interest when peeling PDMS are the force, as well as the existence of any tearing of the material. In order to determine an ideal method of peeling the PDMS, several variables are incorporated. Existing literature shows that the speed of peeling increases the adhesive energy, as used in transfer printing [20]. For automation of peeling, an appropriate peeling speed must be determined to prevent damage to the device. Regarding general peeling properties of adhesive materials, increasing the peel angle (relative to the surface that the material is being peeled from), will decrease the peeling force [29]. This is due to the sharper peel angle of the material reducing the instantaneous area under force. However, peeling PDMS at high peel angle may cause excessive stress in the material. The final variable to be understood is the surface roughness of the mold. Although there will not be considerable variation in mold roughness, investigating the effects of varying roughness will ensure that the previously mentioned variables are adequate for a variety of potential mold surfaces.

To test each of these variables and their interactions, a mold is created containing several pockets for molding PDMS. The Okuma milling machine will be used to automate the peeling process, and the force data is collected at a sampling frequency of 1000 Hz using a three-component piezoelectric force dynamometer (Kistler 9257b). The mold is

attached to the dynamometer using double-sided adhesive transfer tape. Speed of peel and retraction speed are first tested, while keeping the peel angle constant. As a baseline, the peel angle is set so that the pulling force is directly over the peeling edge of the PDMS. In other words, the peel angle is set at 90 degrees, and moved laterally as the PDMS continues to peel. This is achieved by peeling the leading edge of the PDMS along a 45-degree path. The peeling speeds are set at speeds of 0.5 and 5 cm/s. To best record the effects of surface roughness, the mold contains pockets machined at both 127 mm/min as discussed earlier, as well as pockets with a rough ground surface, using a course grinding bit. Figure 12 below is a diagram of the test mold illustrating each variable to be tested.

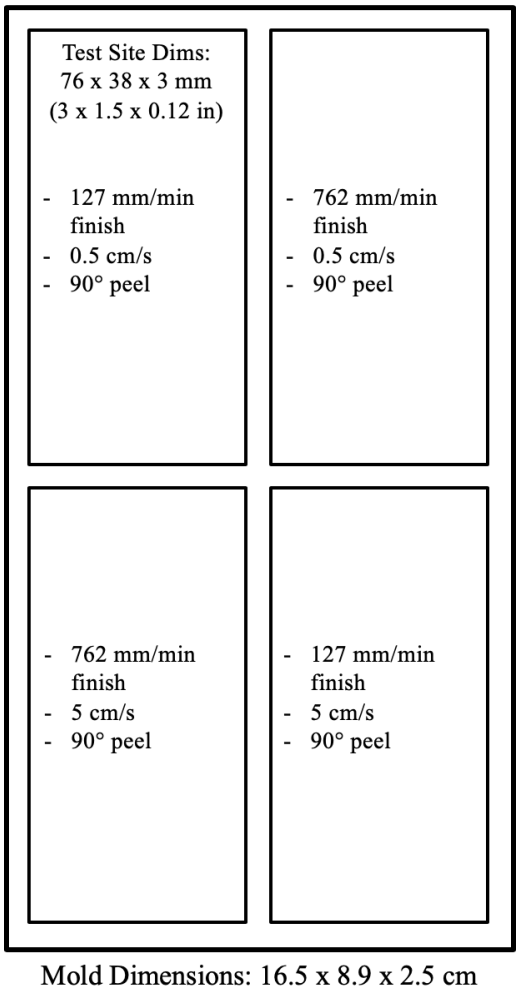

Figure 12 - Testing mold with variables of surface finish, peeling speed, and peel angle

The mold above contains four pockets sized 76 mm x 38 mm x 3 mm (3” x 1.5” x 0.12”). This size allows the four test conditions to fit within the limits of the force dynamometer. Both surface finishes were measured in ten locations to obtain the areal average surface roughness. The milled surface has a roughness of 0.18µm Sq., while the rough ground surface has a roughness of 1.09µm Sq., which is 6.09 times rougher.

To test only the peeling characteristics, the leading edge of the PDMS is manually lifted and attached to the Okuma using a clamp. The CNC machine axes then move so as to produce the desired speed and peel angle while recording the force data. Figure 13 below is an image of the peeling process.

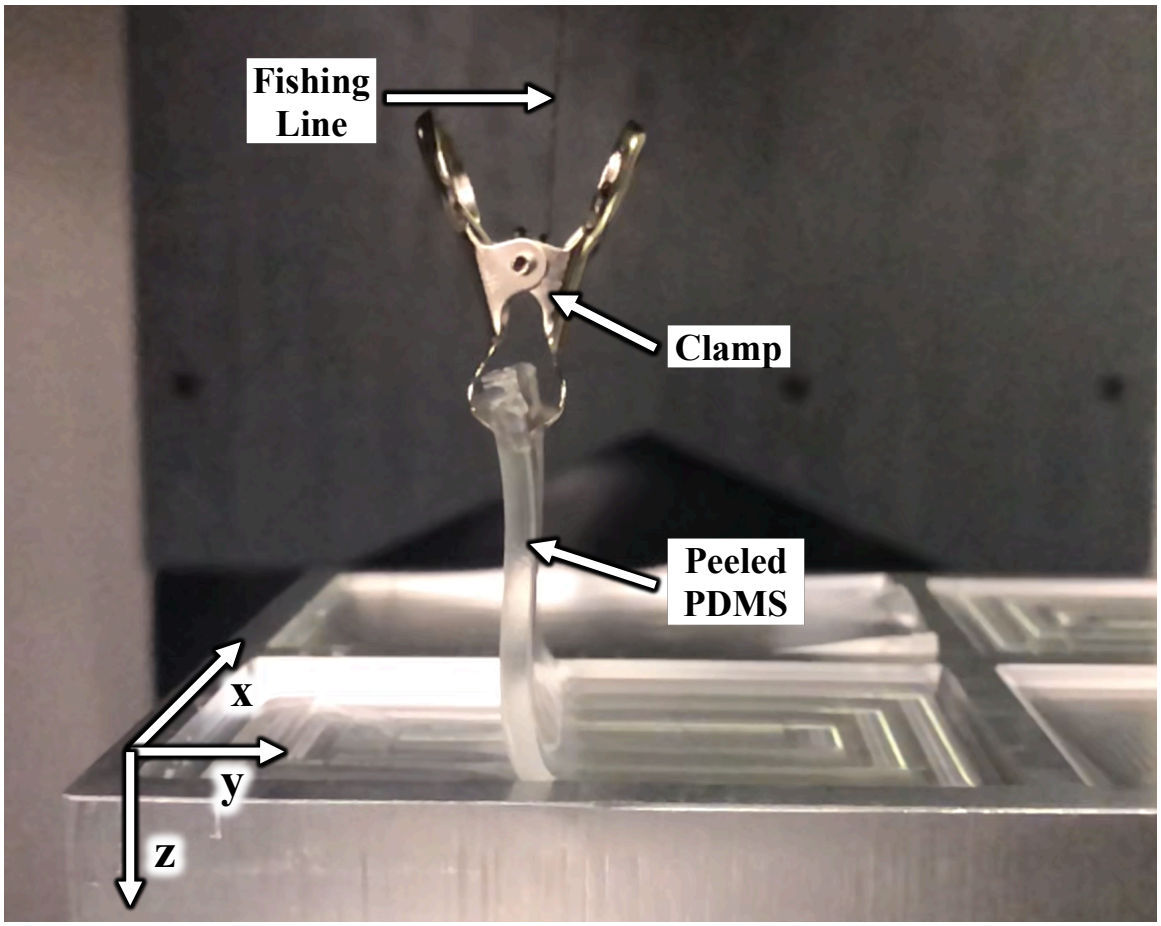

Figure 13 - PDMS being peeled with a clamp on the Okuma milling machine

4.2.1 *Results*

The force dynamometer records forces in the X, Y and Z directions to understand the interaction between the PDMS adhesive forces and the mold. Figure 14 through Figure 17 below show the force measurements of the four peeling tests.

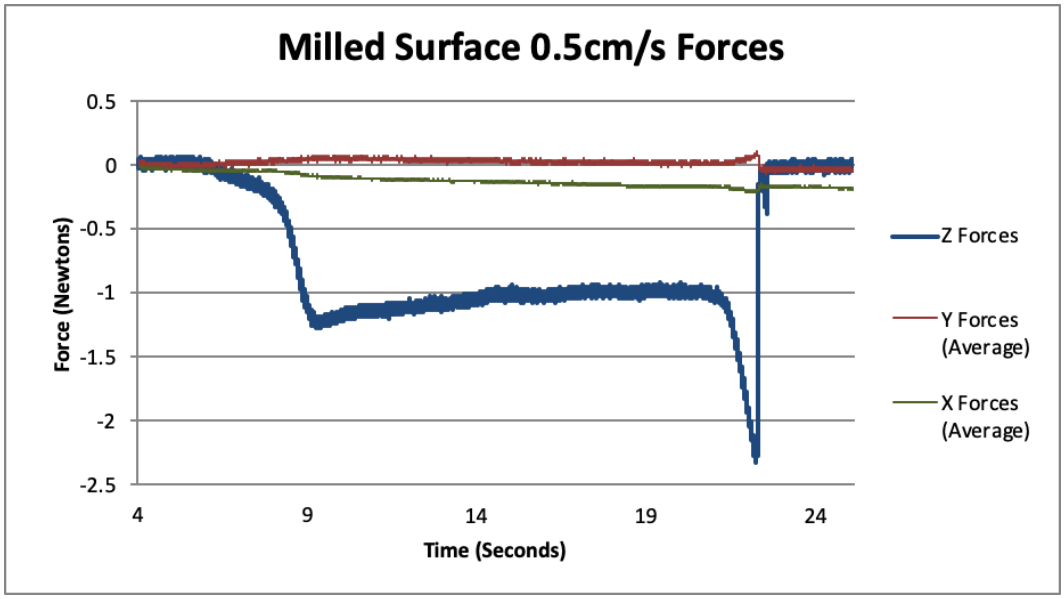

Figure 14 - Force of 0.5cm/s peel from milled surface in X, Y, and Z directions

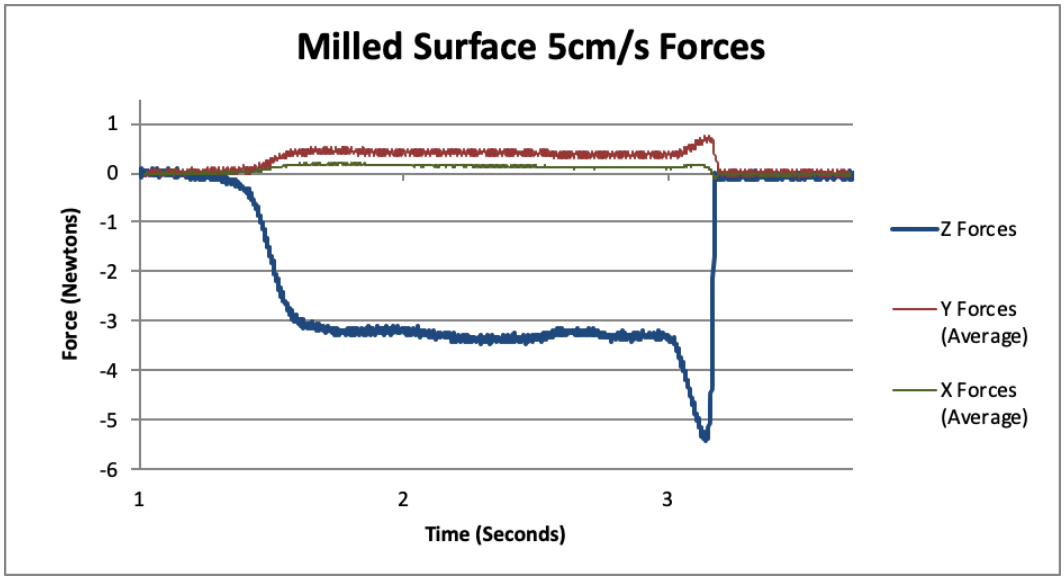

Figure 15 - Force of 5cm/s peel from milled surface in X, Y, and Z directions

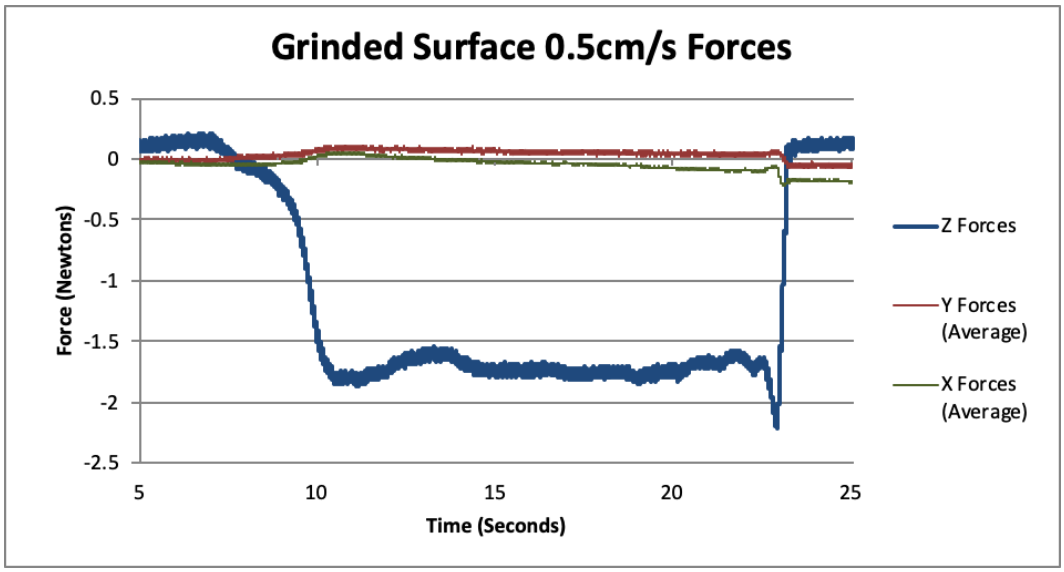

Figure 16 - Force of 0.5cm/s peel from machine ground surface in X, Y, and Z directions

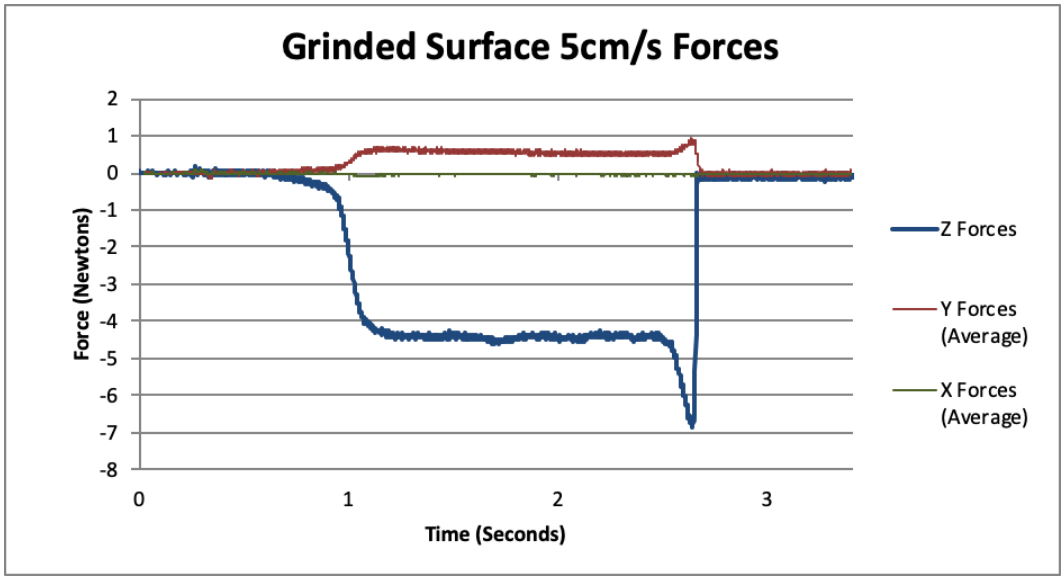

Figure 17 - Force of 5cm/s peel from machine ground surface in X, Y, and Z directions

The graphs show a smooth increase in the force magnitude as the leading edge of the PDMS is lifted upward in the negative Z direction and put under tension. As the peeling is continued along the length of the mold pocket, the force remains constant. Finally, as the trailing edge of the PDMS is lifted from the corner of the mold, adhesive forces are also

present on the back wall of the mold, causing a spike in the force generated. These graphs show that the most significant factor for increasing peeling force is the speed of peel. This agrees with existing literature regarding the increase in release energy as rate of peel increases. As anticipated, a constant 90-degree peel angle generates very little force in the X and Y directions, due to the vertical direction of the force. By increasing the peeling speed by a factor of ten, from 0.5 to 5 cm/s, the force increased from 1.0 to 3.3 Newtons, or 330%. For the ground surface, the peeling force was 1.75 N at 0.5 cm/s, and 4.5 N at 5 cm/s, a 257% increase. These numbers also show the notable increase in peeling force between the milled and the machine ground surfaces. At 0.5 cm/s, the milled surface had 43% less force to peel, and 27% less force at 5 cm/s.

The PDMS did not show any signs of tearing at either peeling speed or surface finish. For final automation of microfluidic device production, it is critical to ensure that all steps are highly reliable, or it will require human oversight, partially defeating the purpose. The forces obtained during testing can be compared to the material properties of PDMS. The polymer has a tensile strength of 2.24 MPa [33]. Given the cross-sectional area of the cured PDMS layer of 38 mm x 2 mm (1.5” x 0.08”), the PDMS can withstand 173 N of peeling force. This is significantly higher than the maximum force of 6.8 N experienced by the trailing edge of the PDMS when peeling at 5 cm/s on the machine ground mold.

These experiments indicate that no significant damage to the PDMS layer will occur due to excessive forces during peeling. This ensures that progress can be continued toward specific robotic methods of removing the PDMS. Although large scale damage to

the PDMS will not occur, characteristics associated with the removal methods may introduce additional stresses on the material.

4.3 Embedded Peel Tab

It has been shown that continued peeling of the PDMS is amenable to automation. However, in order to automate the entire removal process, the robot must be able to reliably initiate the peel using a simple technique. One of the most fundamental concepts is to embed an apparatus (e.g. peel tab) into the PDMS, which could be handled by the robot. The embedded peel tab should be simple in its design, allowing for prototyping using 3D printing. The tab can be disposable, by trimming the excess PDMS from the layer. For this idea to work, the tab would need to be placed in the uncured PDMS, resting on the bottom of the mold pocket. Columns from the base of the tab would extend through the PDMS to allow a robot to grip, while also ensuring the tab remains embedded in the PDMS. Figure 18 below shows an implementation of the peel tab idea.

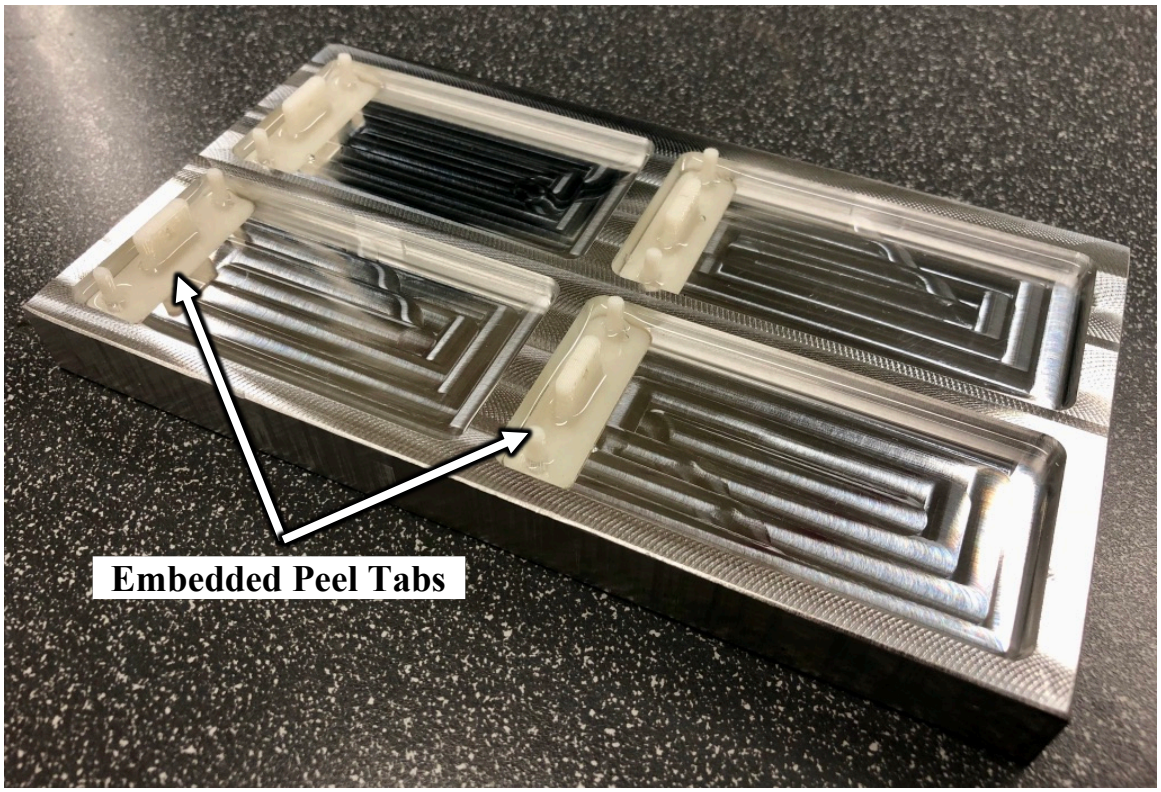

Figure 18 - Embedded peel tabs in a mold with cured PDMS

The chamfer tabs are slightly less than 38 mm (1.5”) long to fit the width of the mold, and are 12.7 mm (0.5”) wide. The Okuma CNC milling machine was again used to automate the peeling process, with the piezoelectric force dynamometer recording the peeling forces. A fifty pound-test fishing line was used to attach the peel tabs to the CNC spindle. The CNC milling machine would then peel using the same 45-degree path as before.

4.3.1 *Results*

During a peeling speed of 0.5 cm/s, 80 N of force was experienced, resulting in the adhesion force of the transfer tape being exceeded. The tab showed no signs of separating from the mold. After analysis, it was determined that a thin layer of PDMS under the tab

generated a significant amount of adhesion. Although there are methods to prevent PDMS from traveling under the tab, such as incorporating a rubber coated bottom, this would be impractical for large scale usage.

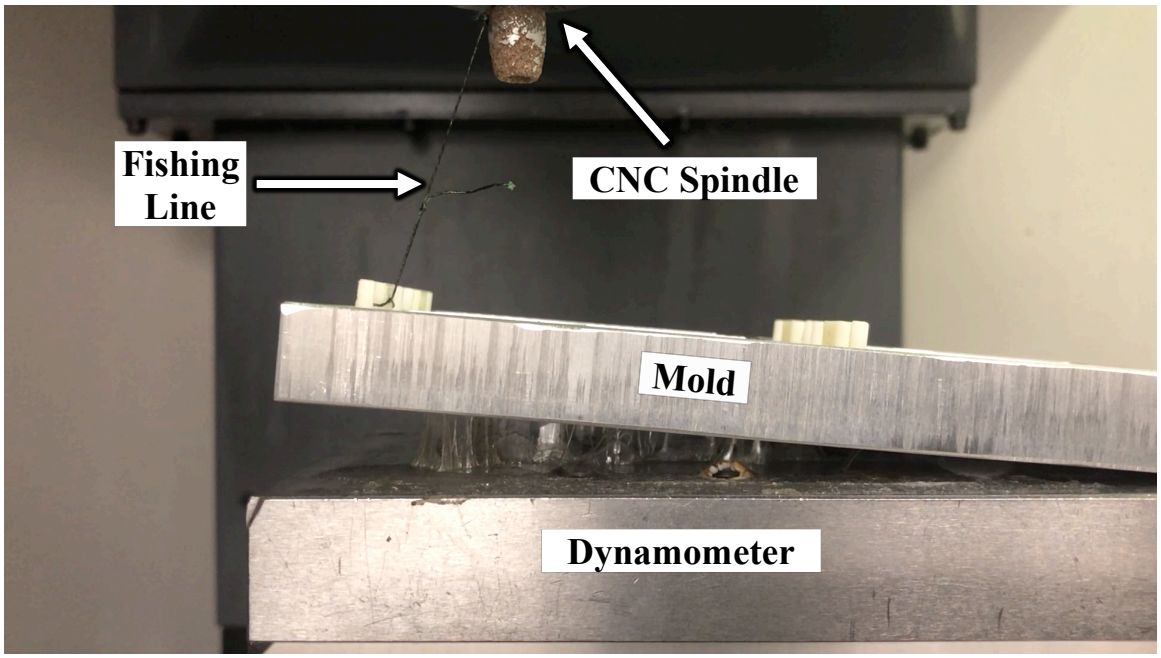

Figure 19 - Embedded tab failed peel due to excessive PDMS adhesive forces, causing the mold to lift up from the dynamometer

The reason that the tab generates so much more adhesive force than the continuous peeling as before is due to the larger surface area under tension. During continued peeling, only one edge of PDMS is experiencing an adhesive force, which allows for easy propagation of the peel. In contrast, the rigid tab creates adhesive forces throughout the entire bottom area of the tab, regardless of the angle of peel.

4.4 Chamfer Tab

The peel tab showed that there is considerable adhesion across the bottom area of the tab. When the tab is pulled in a direction normal to this adhesion, the force that can be

withstood exceeds the limitations of the equipment. To allow for propagation, the peeling force must be applied outside the perimeter of the PDMS layer. Additionally, the peel must start along a top outer edge of the PDMS, rather than at the bottom of the mold. To enable this, a chamfer-walled mold will allow the peel to initiate along a top edge of the PDMS, and travel across the surface of the pocket until the tab has been completely peeled from the mold. Chamfer tabs with a corresponding shape are placed in the mold prior to pouring the PDMS. After peeling of the tab has occurred, the PDMS will act in a similar manner to the earlier continued peeling experiment with the clip. Figure 20 below shows the chamfered walled mold with chamfer tabs embedded inside the PDMS layer.

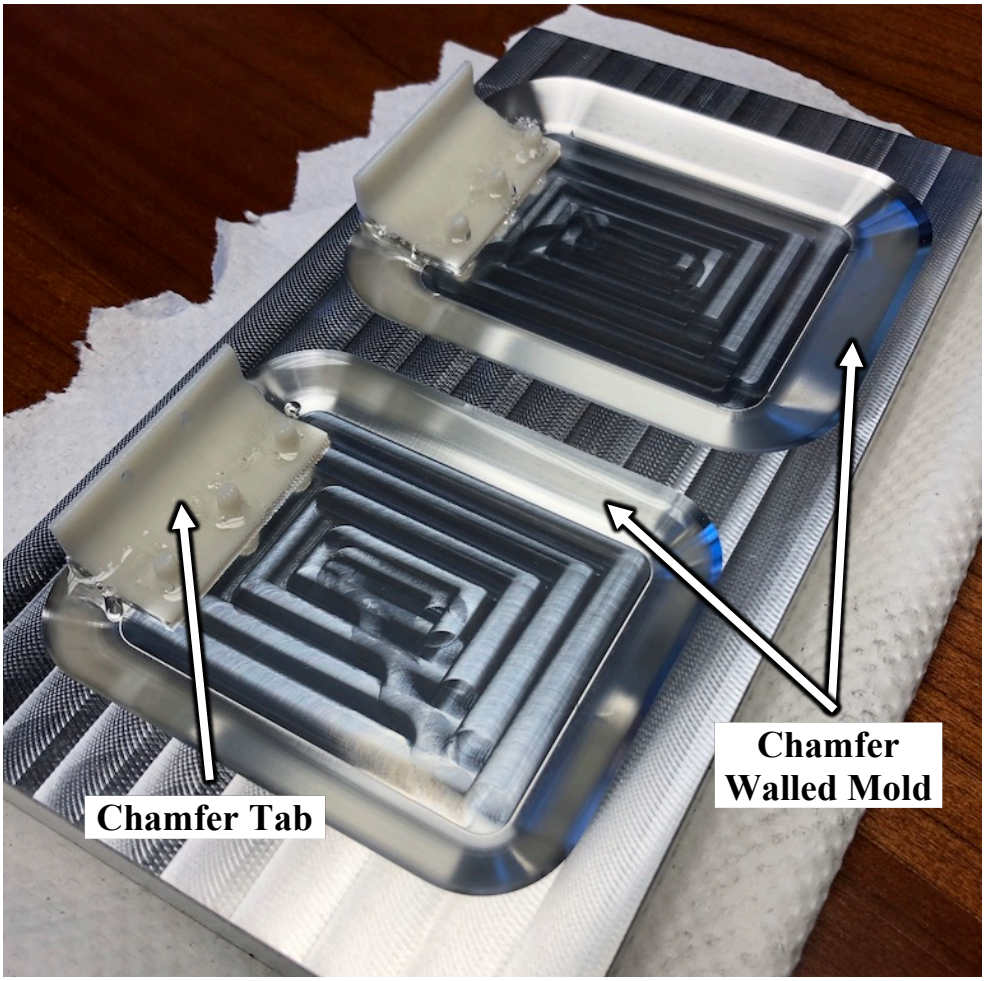

Figure 20 - Chamfer walled mold with embedded chamfer tabs

The automated peeling action realized earlier on the CNC milling machine was replaced with a Universal Robotics UR5 robot. Force data was recorded using an ATI Gamma Force/Torque Sensor mounted between the tool center point (TCP) and the end-effector of the robot. As with the CNC milling machine, a fishing line attached the chamfer tab to the robot end effector. A peel path of 45 degrees was also used again.

4.4.1 *Results*

The peeling experiment was performed twice, resulting in one successful peel, and one unsuccessful peel. The successful test performed as intended, initiating the peel at the outer edge of the tab and PDMS. A thin residual layer of PDMS between the tab and mold remained bonded to the metal mold. In the second test, the tab was cured with additional space between the mold, thereby increasing the amount of PDMS underneath. During the peeling attempt, the tab was unable to peel away from the additional PDMS underneath, which resulted in the tab tearing out of the PDMS. Figure 21 shows the failed chamfer tab peel test.

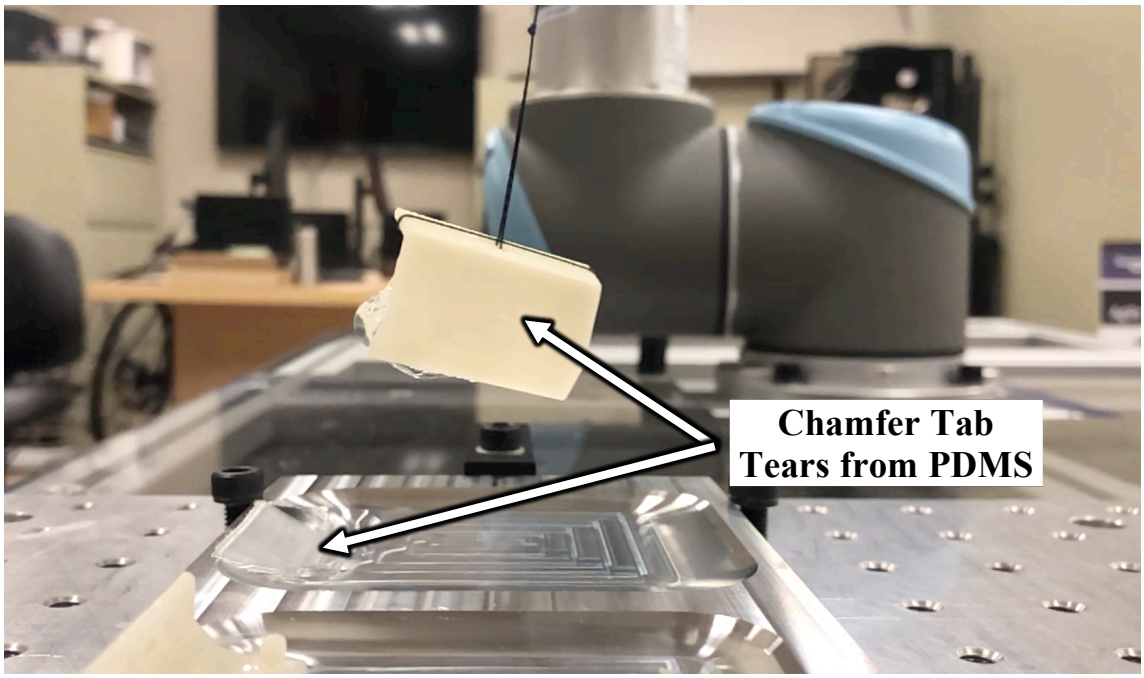

Figure 21 - Failed chamfer tab peel test due to excess PDMS under the tab

The tests show that with the correct positioning of the chamfer tab, this method can be successful. However, this would require additional automation steps to ensure the tab remains in the correct position throughout the curing process. This would likely require an apparatus to hold the tabs in place.

Although the chamfer tabs could be an effective method to automate the PDMS layer production process, there are undesirable drawbacks. The disposable aspect of the tabs would require an additional manufacturing process to create the tabs. As mentioned, the robot would need to perform the additional tasks of placement and fixturing of the tabs. Lastly, the disposable tabs would need to be trimmed prior to assembly and bonding of the device. Although the use of disposable tabs would have advantages over the current manual production process, other methods were investigated in an attempt to optimize the automation. A more refined method should incorporate reusable and/or generic equipment, to minimize frequent custom manufacturing, which would increase overall costs.

4.5 Bladed Gripper

Earlier experiments in this chapter showed that when peeled progressively, PDMS exhibits small adhesive forces. These understandings were combined with the current method of peeling by using a sharp blade, to create a more automation-friendly approach. After manually cutting the PDMS, the blade is used to lift and peel one edge of the PDMS, which requires visual manipulation. Instead, a robotic gripper can be incorporated to both lift and clamp the PDMS. The bladed gripper is a custom attachment for a robotic gripper. The gripper is designed with a sharp plastic blade attached to the leading end of the lower gripper arm. This blade travels down the chamfered wall of the mold, cutting the PDMS from the mold. After adequate travel under the PDMS, the robotic gripper clamps down, pinching the PDMS between the lower blade, and upper arm. Figure 22 shows the bladed gripper set up for a peeling test on a chamfer-walled mold.

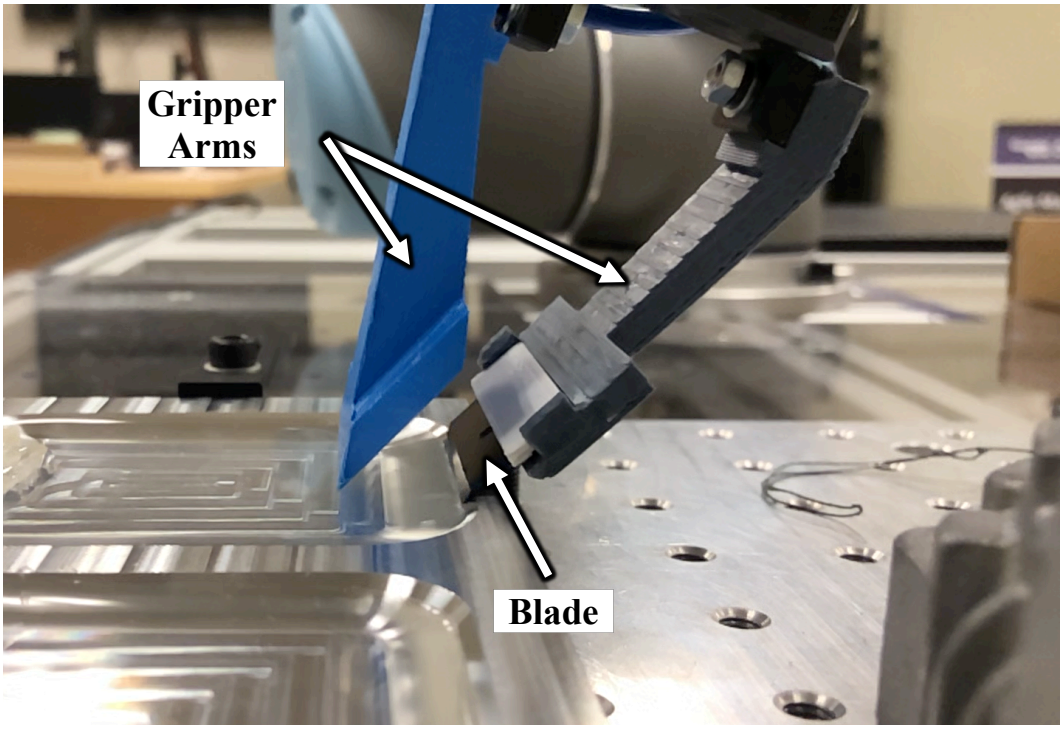

Figure 22 - Bladed gripper before peel test on chamfer-walled mold

4.5.1 *Results*

An experiment was run by programming the robot end effector to slide down the chamfer wall. However, rather than the blade sliding under the PDMS, it directly pierced part of the PDMS. This prevented the PDMS from peeling, and instead generated enough force to break the gripper. This showed that the alignment of the gripper with the mold must be perfect to enable the blade to only slide under the PDMS layer.

Due to natural manufacturing tolerances and variations in the positioning of the gripper and the mold, modifications would be needed to increase reliability. This could be accomplished with a blade that has a small amount of flexibility to account for these variations. During testing, however, it was found that the adhesion between the top surface of the blade and the PDMS can cause difficulties in peeling. This finding, combined with challenges in programming the blade to follow the chamfered wall of the mold, shows that a bladed gripper may be inadequate for final automation.

4.6 Insert Gripper

The benefits of the bladed gripper combined with the success and findings from the chamfer tab were used to generate the concept of an insert gripper. The insert gripper has a detachable lower gripper finger, which is embedded in the PDMS similar to the chamfer tab. The robot gripper is then maneuvered to interlock with the lower finger. With the top and bottom gripper fingers, it pinches the PDMS and peels. The benefit of the insert gripper over the chamfer tab is that the columns on the tab would no longer be needed to assist in lifting the PDMS. These columns, intended to prevent the tab from separating from the PDMS, would be replaced by pinching the PDMS. The result of this would allow the insert

gripper to be removed after peeling, rather than being trimmed and discarded. Figure 23 is a CAD model of the insert gripper.

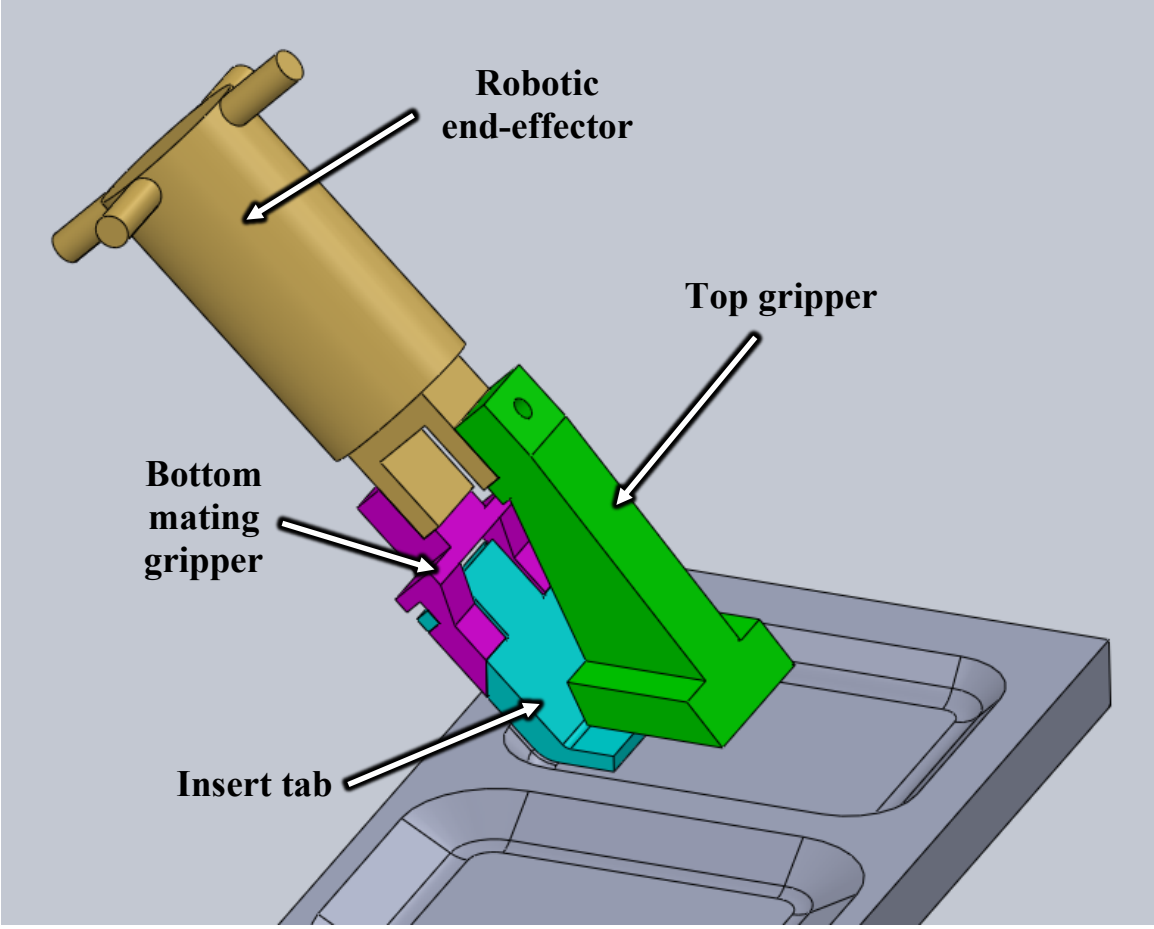

Figure 23 - Insert gripper CAD model consisting of robotic end-effector, insert tab, bottom mating gripper, and top gripper

While the insert gripper would have the advantage of reusability over the tabs, there is still the difficulty of positioning the insert throughout curing. Additional challenges include mating the robot to the insert gripper, as well as separating the insert gripper from the PDMS. For large scale automation, the insert gripper is not ideal due to these complexities and was therefore not investigated further.

4.7 Summary

This chapter discussed several methods investigated in an effort to peel a cured PDMS layer from a machined aluminum mold. The most significant finding was the adhesive characteristics of PDMS, and the importance of minimizing the surface area of bonded PDMS that is subjected to a peeling force. PDMS naturally peels with a low force of 1-4 N, much below the tensile strength of the polymer. However, as the surface area under load increases, such as the area under a peel tab, the force to de-bond that area can be larger than the tensile strength of the material, resulting in tearing but no peeling. When attempting a method similar to the manual approach, the bladed gripper showed the difficulty in attempting to replace human manipulation with a robotic motion. While manual methods use blades to cut and lift the PDMS, humans can visually determine the success of a cut. In contrast, robotic automation would have to rely on a high success rate with a single pass of the blade, which was determined to be an unrealistic goal. These methods discussed could be combined into a gripper with a mating embedded tab. This approach would allow for the reusability, along with the successful findings from the chamfer tab. While this could be a successful method of peeling, the additional tasks required for correct placement of the insert gripper make this method less than ideal for final automation.

CHAPTER 5. DE-BONDING AND PEELING PDMS

5.1 Introduction

Chapter 4 explained the adhesive forces of PDMS, and how it creates challenges in removing it from the metal mold. The main difficulty in automation was determined to be the initiation of the peeling process, due to the challenge of focusing the force on the PDMS to a very small region, such as a single edge. This is especially true when attempting to perform the peeling initiation process with simple robotic motions. Rather than peeling the PDMS in one step, a de-bonding process is required to first reduce the adhesion between the PDMS and the mold prior to the peeling process.

The concept of de-bonding using air pressure has been previously used, as discussed in existing literature. Researchers have inserted air tubes after creating a hole in the PDMS with a biopsy punch [25]. However, the process of piercing the PDMS for air de-bonding has not been studied. With reduced adhesion due to de-bonding, the peeling process can be initiated and the PDMS removed for final device assembly.

This chapter will cover air needle de-bonding, followed by a suction peel. The de-bonding is intended to reduce or eliminate adhesion between the mold and the PDMS. Previous literature showed that de-bonding PDMS with air requires about 50 psi, which is greater than the maximum pressure achievable by a perfect vacuum (-14.7 psi) [25]. In order to prepare adequate de-bonding for suction peeling, specific steps and techniques will be discussed.

5.2 Air Needle De-bonding

It has been shown in prior work that introducing pressurized air between PDMS and the bonded substrate is successful in de-bonding. Mechanical devices, as described in Chapter 4, alter the natural peeling process of PDMS, by increasing the surface area and introducing additional adhesive forces. Instead, the use of pressurized air allows the PDMS to de-bond by expanding concentrically as the air travels. Peeling along a single curved edge exhibits similar dynamics, which allows for the continued peeling of PDMS with low force as shown earlier in Figure 14 and Figure 15.

While experimenting with peeling methods in Chapter 4, it was observed that after initially separating the PDMS from the mold, adhesion is significantly reduced. An air de-bonding process can reduce these adhesive forces and allow automation to completely remove the PDMS layer. The use of pressurized air introduced through holes in the bottom of the mold were considered for air de-bonding, but were not carried out due to complexity of the overall system design. In addition, if holes are machined into the mold PDMS may enter and block the holes prior to curing. Creating holes small enough to potentially prevent PDMS from flowing through may present challenges in tooling and machining. Lastly, an apparatus would be required to direct the pressurized air supply through the mold.

Rather than introducing air through the mold, a more cost-effective method would be to insert a needle into the PDMS until it makes contact with the mold. Pressurized air could then be introduced between the PDMS and the mold surface via the needle, causing de-bonding of the PDMS similar to the method discussed in the existing literature [25].

5.2.1 *Needle Characteristics*

Given that the final targeted market of microfluidic device automation includes small laboratories with limited budgets, selecting ready-made equipment when possible is preferred. Reducing custom supplies will allow for lower costs, and simplified maintenance. For these reasons, hollow dispensing needles of various gauges and tip shapes, flat and chamfered, are investigated. Initially, the metrics of interest are the force required to pierce the PDMS, as well as the ability to completely penetrate through the PDMS to the surface of the mold. Ultimately, the objective of the experiments is to maximize the de-bond area to improve the reliability of peeling via a suction cup.

The air needle sizes chosen for experimentation range consist of readily available standard gauges. Gauge 14 is the largest diameter (dia.) disposable needle that is commonly available, with a diameter of 2.11 mm. The smallest diameter needle that is typically available is gauge 22, which is 0.72 mm in diameter. Other needles tested to determine the ideal diameter include gauges 16 (1.65 mm dia.), 18 (1.27 mm dia.), and 20 (0.91 mm dia.). All needles use a threaded adapter (LUER lock), which is common for syringes, as it is leak free. The shape of the needle tip may also affect the piercing force. To address this variable, each needle gauge is tested with a blunt (or flat) tip, as well as with a chamfered tip.

Figure 24 - Flat and chamfer tip needles. Gauge sizes from left to right are 14, 22, 16, 20

In order to record the force of piercing, the needles must be mounted to the robotic end-effector. A 3D printed attachment was designed to bolt to the robot's tool plate. The attachment is integrated with a series of fittings to connect the air supply to the needles. Figure 25 shows the robot with the needle attachment end-effector.

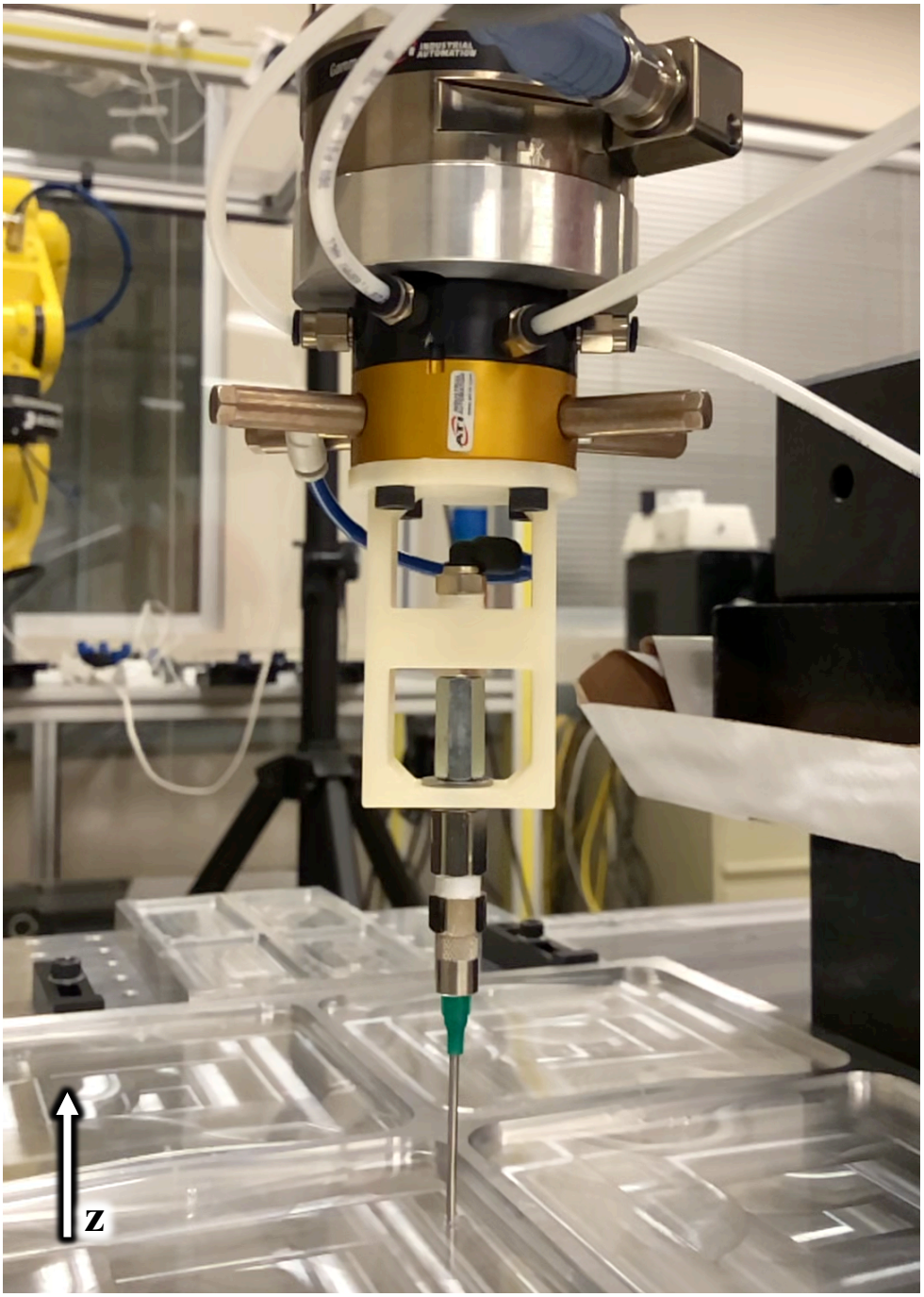

Figure 25 - Needle robot attachment with 14-gauge needle

With the needles attached to the robot, the ATI Gamma 6-axis force sensor mounted to the tool flange can record the forces required to pierce the PDMS. Piercing forces are obtained by teaching the robot to follow a trajectory downward, in the negative

Z direction indicated in Figure 25, at a slow velocity of 1 mm/s. The robot is lowered using a velocity-stop controller, which stops the robot's motion when a force that exceeds the set value is detected. The flat tipped needles were first tested, piercing the PDMS vertically, normal to the surface of the mold. Each needle gauge required a similar force to pierce the PDMS, however, thinner gauge needles were susceptible to bending under the compressive force. This lack of rigidity is highly undesirable, due to reduced durability and the safety concerns associated with a failed needle. Figure 26 and Figure 27 show the piercing forces recorded using a 14-gauge flat-tipped needle when the velocity-stop was set to 35 N and 70 N, respectively.

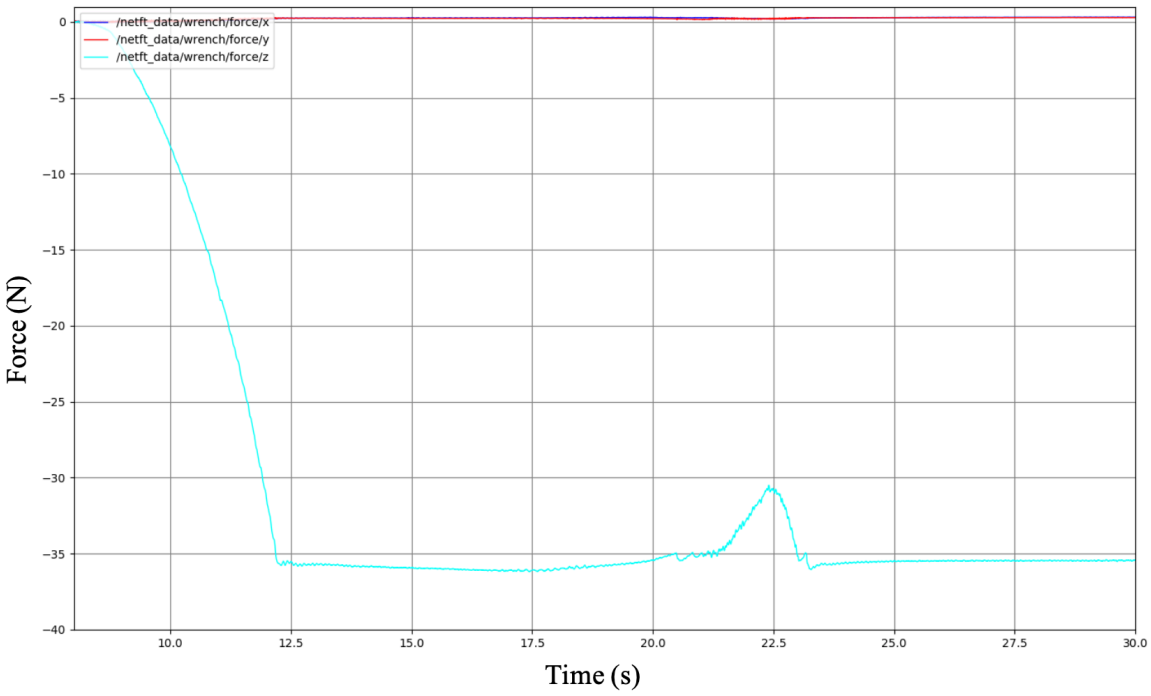

Figure 26 - Piercing force with velocity-stop set to 35 N

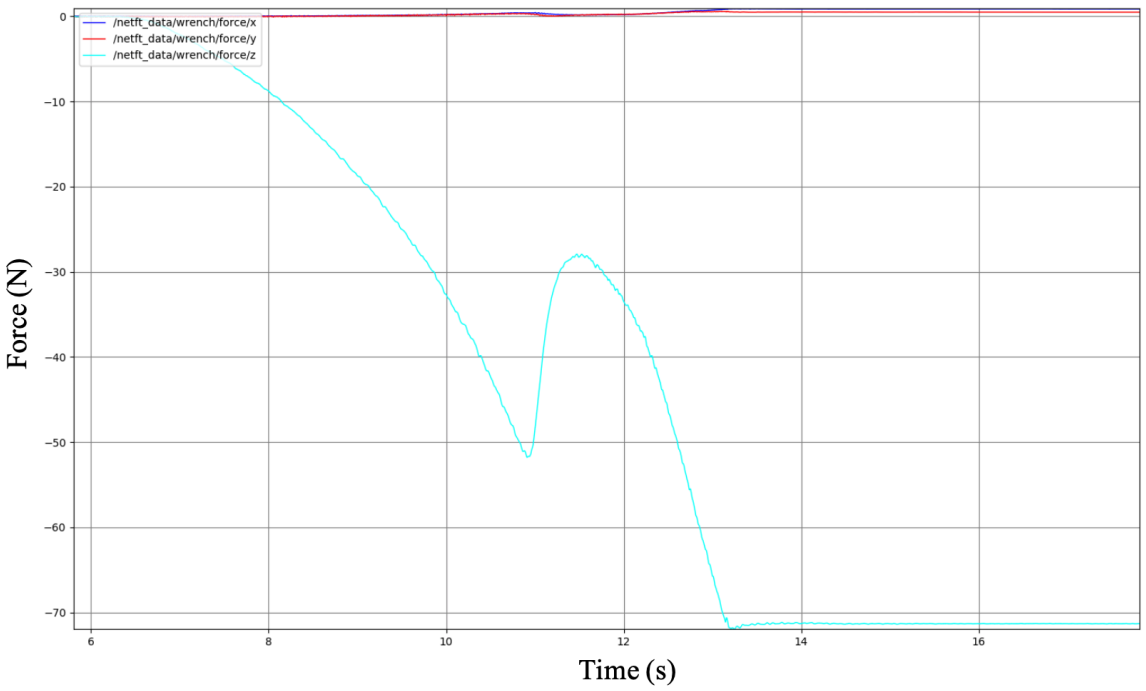

Figure 27 - Piercing force with velocity-stop set to 70 N

Figure 26 shows the force halts at 35 N for approximately 8 seconds (from the time of 12 seconds to 20 seconds) before dropping to about 31 N until the needle contacts the bottom of the mold, after which the force increases to 35 N again. In contrast, when the velocity-stop force is set to 70 N in Figure 27, the piercing force reaches 50 N, before dropping to about 29 N until the bottom of the mold is reached. During the time the force is maintained at 35N, the velocity is zero (or very near zero). These graphs show the elastic properties of PDMS, and how velocity affects the piercing force. In Figure 26, the needle is nearly stationary as the PDMS slowly tears under the force of the needle tip. In Figure 27, the needle continues at a velocity of 1 mm/s throughout the piercing (due to the velocity-stop threshold not being met), which generates an additional 15 N to initiate piercing. However, once piercing of the PDMS begins, the experiments show that a constant force of about 30 N +/- 1 N is required to continue piercing the PDMS. Throughout

the experiments, neither the 14-gauge needle, nor robot attachment was damaged. This allows for a higher selected force to be input into the velocity-stop program, to ensure complete contact of the needle with the bottom of the mold.

Piercing force of the chamfer needles were also tested to enable later experimentation of de-bond area. Given the angled tip of the needle, the robot must pierce the PDMS at the corresponding angle so that the needle tip is flush with the surface of the mold. However, as shown in Figure 28, the needle bends as it makes contact with the surface of the mold, rather than arresting the needle motion.

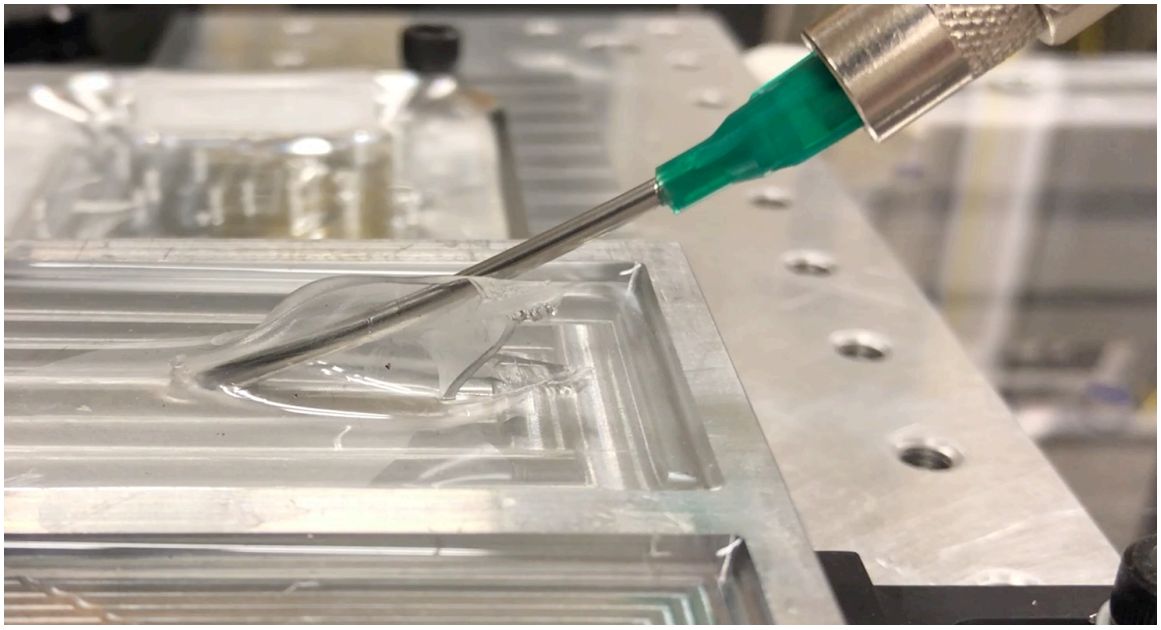

Figure 28 - Chamfer needle bending after making contact with mold

While the needle could be reinforced to prevent bending, it is impractical, given that the force to pierce is nearly identical to the flat tipped needle. Additionally, the chamfer needle is less safe, so it will not be used for de-bonding.

With the piercing forces determined, testing of de-bond area was begun. Preliminary tests were first performed to understand the characteristics of de-bonding. This

initially included testing of the different gauge needles. Gauge 18 (1.27 mm dia.) was the smallest diameter needle that did not exhibit significant bending under load. The de-bonding characteristics of the 18-gauge was compared to the 14-gauge (2.11 mm dia.) needle. During experimentation, the smaller needle resulted in less area de-bonded. This can be attributed to the lower flow rate of air given the smaller cross-sectional area. These preliminary tests were able to eliminate the use of all chamfer needles, as well as smaller gauge flat needles. Moving forward, only the 14-gauge flat-tipped needle was used. While the de-bonding characteristics of this needle are superior, it is also more durable and safer due to its larger dimensions and non-sharp features.

5.2.2 *De-bonding Variables*

With the 14-gauge flat needle chosen for all future testing, variables with potential impact on the de-bonding area were determined. The first variable to be included was the location of the needle piercing. An understanding of needle placement must be determined for automation of any sized mold. In order to de-bond the PDMS, the needle must be lifted slightly off the bottom of the mold to allow air to flow. This introduces another variable of retraction. The retraction can either be a certain distance upward, or a continuous retraction at a set velocity.

Preliminary tests were conducted to investigate a continuous retraction speed versus a retraction that pauses at a set height. A height of 3 mm was chosen to ensure the PDMS is lifted slightly by the needle to assist in directing air underneath. Various retraction speeds, ranging from 1 mm/s to 100 mm/s, were also evaluated in preliminary tests. These tests were used to narrow down a range of appropriate needle retraction conditions prior to systematic experimentation. The most significant finding from adjusting the retraction

distance was the symmetry of the de-bonded area. The PDMS de-bonds from air pressure by inflating and lifting upward, which propagates the peel concentrically outward. If the PDMS balloons upward faster than the retraction rate of the needle, the adhesion between the needle will slightly anchor the PDMS downward. This forces the de-bond to lose symmetry, directing more air in a certain direction. The direction of the de-bond is largely random, affected by slight variations in the retraction of the robot, and flexibility of the needle and fitting. Figure 29 is an image of the PDMS being lifted upward via air pressure as the needle is retracted.

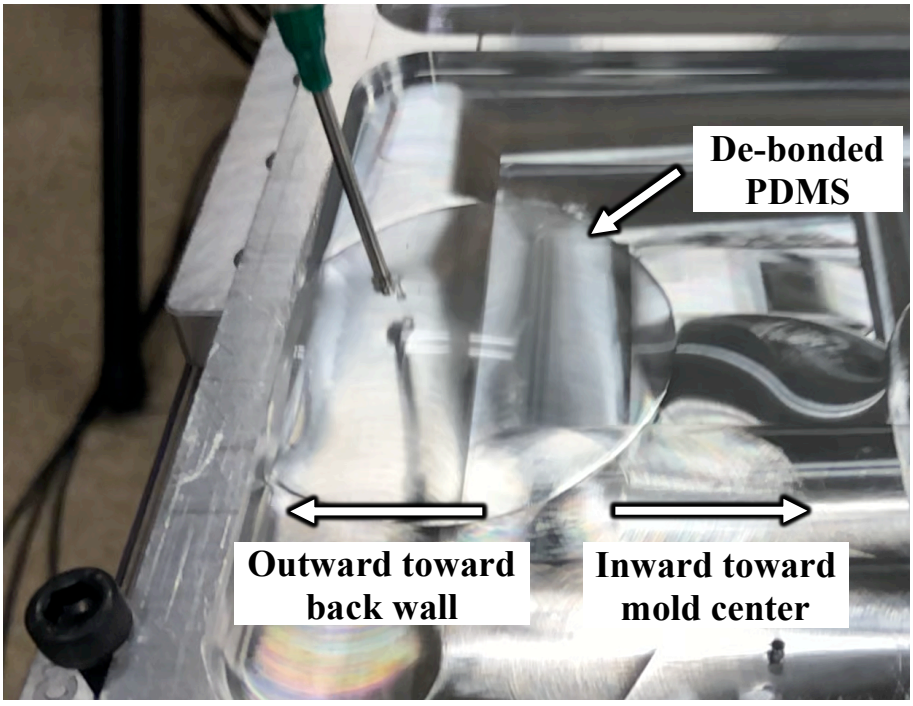

Figure 29 - Image of needle de-bonding PDMS upward via air pressure. Inward and outward mold directions specified for future reference.

Initial testing showed that varying the retraction speed generally results in similar de-bonding areas, due to the de-bond occurring almost instantly after the needle detaches from the mold. However, speeds around 10 mm/s and less resulted in anchoring the PDMS

downward as discussed above. Speeds around 80 to 100 mm/s or greater are too fast, reducing the ability for maximum de-bonding before the needle exits the PDMS.

For current manual methods, PDMS is first trimmed around the perimeter to remove the meniscus at the wall. The presence of a meniscus prevents proper stacking of PDMS layers due to the lack of flatness required for proper bonding. In order to eliminate this issue for final automation, a chamfer-wall mold can be incorporated, which moves the meniscus outside of the perimeter of the stacked device above.

To test the variables of needle placement, retraction speed, and vertical versus chamfered wall, a mold containing 8 pockets was machined. Four pockets contain vertical walls while 4 have chamfered walls. Each wall type is tested with needle placements of 5 and 15 mm inward from two adjacent corners, at retraction speeds of 20 and 60 cm/s. Figure 30 is a diagram of the mold with the testing plan.

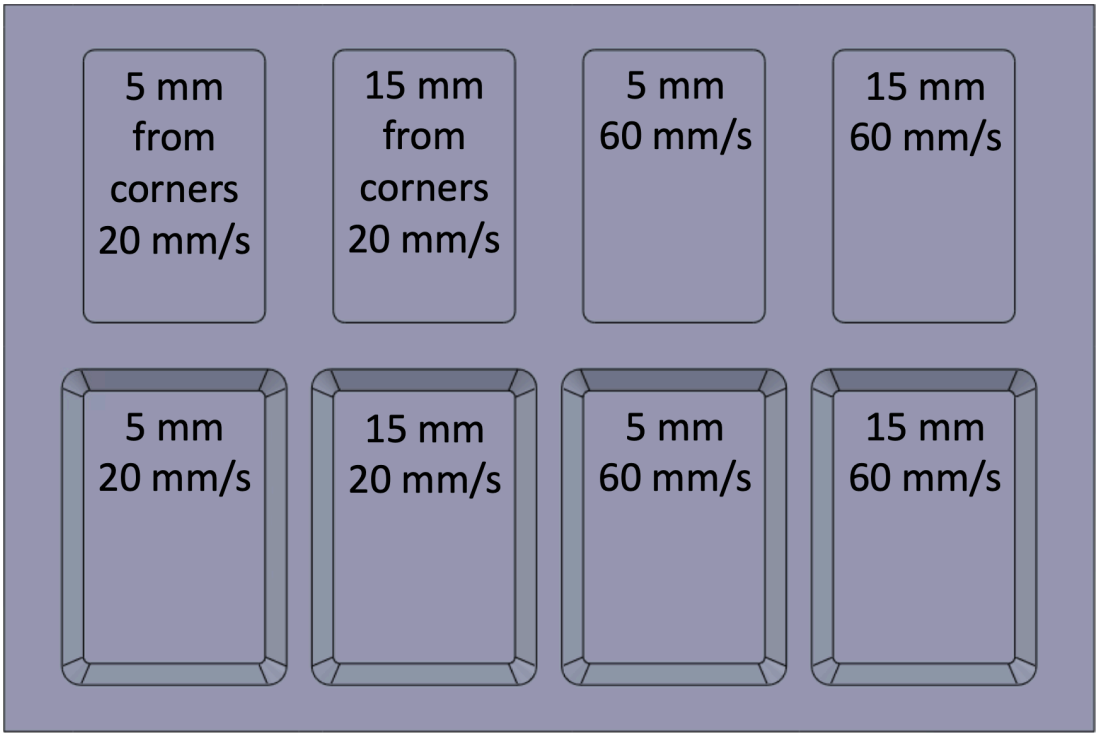

Figure 30 - Experimental mold for testing effects of needle placement, retration speed, and vertical vs. chamfer wall

The experiment was conducted using the UR5 robot, which was programmed through the teach pendant. The piercing force was controlled using the Z-axis coordinate of the robot, programming a slight interference between the needle and mold, which results in an opposing force. The height of the needle was set so that approximately 70 N was generated when the needle contacted the mold. The tests were conducted using high speed video to best understand the interaction between the variables and the resulting de-bond area.

Prior work reported in the literature found that 50 psi of pressure is required to de-bond PDMS, after which the de-bond occurs rapidly [25]. Using this result, a pressure of 60 psi was used to ensure de-bonding, while also remaining at a practical pressure obtainable by affordable compressors.

5.2.3 *Results*

The main finding was the difference in de-bond area between the vertical and chamfer wall molds. De-bonding stops once any portion of the area reaches an opening to atmospheric pressure. Once this occurs, that pathway is of the least resistance, preventing further de-bonding. The vertical wall mold requires that pressure builds up enough to overcome the shear strength of the adhesive bond, given that the edge of the PDMS must lift upward, and therefore parallel to the vertical wall. In contrast, a chamfer wall mold can allow for propagation of the de-bond from the bottom of the mold, and then upward along the wall, which greatly reduces the resistance of the air to escape the nearest wall. Figure 31 and Figure 32 compare the area de-bonded due to the air pressure of vertical versus chamfer wall molds.

Another significant finding was the peeling caused by the adhesion between the needle and the PDMS. At the slower retraction speed, the adhesion allowed for significant additional peeling following air de-bonding. Although this can be considered advantageous, it is unreliable as it is not the intended purpose of the air needle. This adhesion could be dramatically affected by PDMS thickness, extent of cure, and the presence of liquid/lubricant. Figure 32 and Figure 33 show the comparison between the initial air de-bonded area and the final de-bonded area caused by needle adhesion, just prior to the needle separating from the PDMS. The difference in the areas between these two images is strictly due to the peeling caused by the adhesion of the needle to the PDMS during retraction.

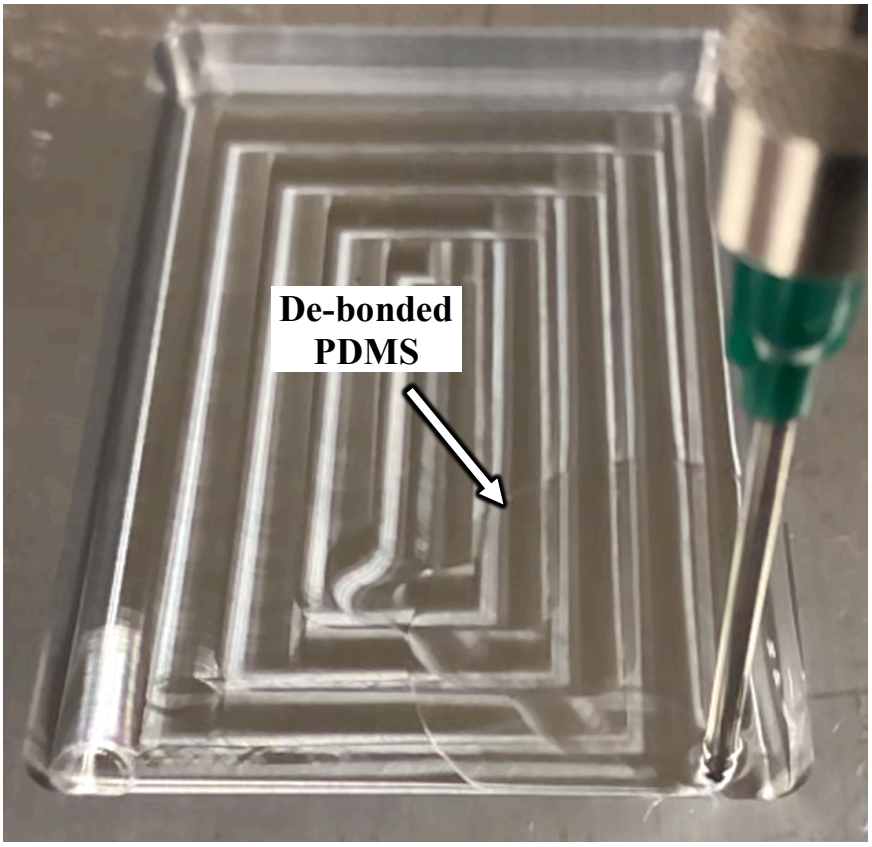

Figure 31 - Area de-bonded from air pressure alone on vertical wall mold. Needle conditions are 5 mm inward from the corner, with a retraction speed of 20 mm/s

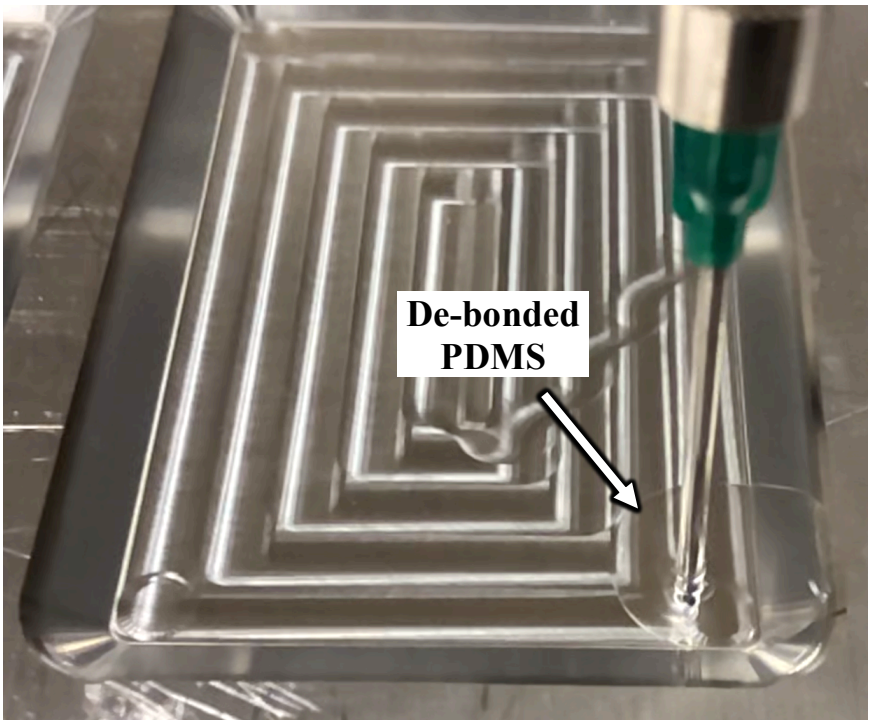

Figure 32 - Area de-bonded from air pressure alone on chamfer wall mold. Needle conditions are 5 mm inward from the corner, with a retraction speed of 20 mm/s

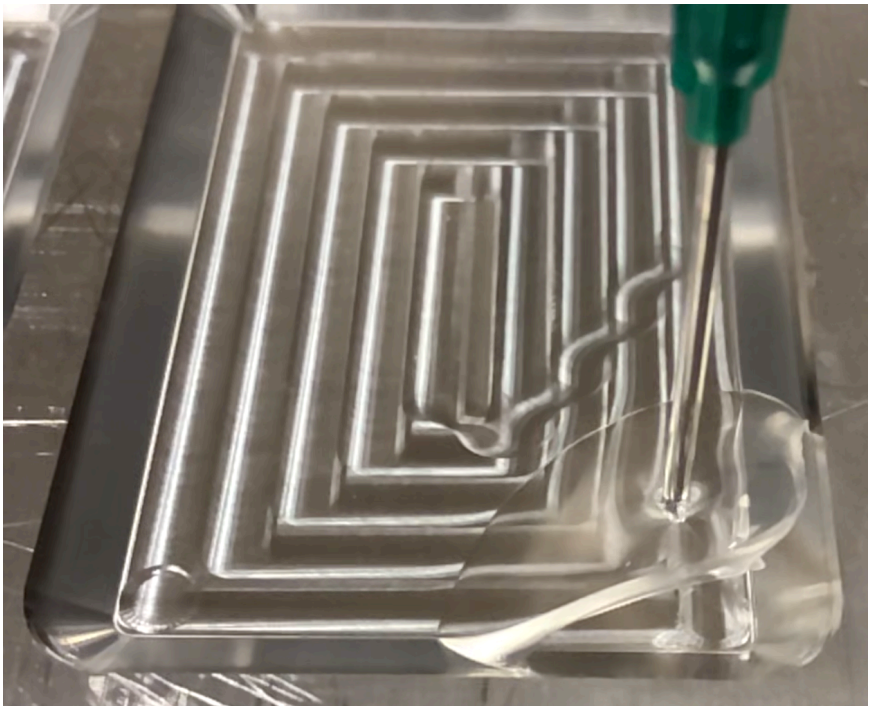

Figure 33 - Area de-bonded from air pressure and needle peeling on chamfer wall mold, following needle retraction in the figure above.

The placement of the needle also has an effect on the de-bond area. As discussed earlier, de-bonding continues until the pressurized air escapes one edge of the PDMS. When the needle is placed further inward from the perimeter of the PDMS, the air must travel further, ideally in all directions, to reach an edge. Therefore, the needle location of 15mm inward resulted in more de-bonding than the 5mm location.

These experiments used two needle locations in an attempt to de-bond the full width of the mold. However, de-bonding stops once it reaches previously de-bonded PDMS, or an outer edge, whichever comes first. Therefore, two overlapping needle de-bonding sites will generally not double the area, especially if placed near each other. This can be seen in Figure 34, where the second needle piercing on the right de-bonded little additional PDMS towards the right of the needle. This is due to the first needle location on the left de-bonded very close to where the right needle was later placed. Alternatively, if the needle locations are too far apart, there will be two separate de-bonded areas, with bonded PDMS in between. This will not assist in peeling the PDMS, as the bonded areas will prevent initial lifting. Figure 35 shows these separate de-bonded areas.

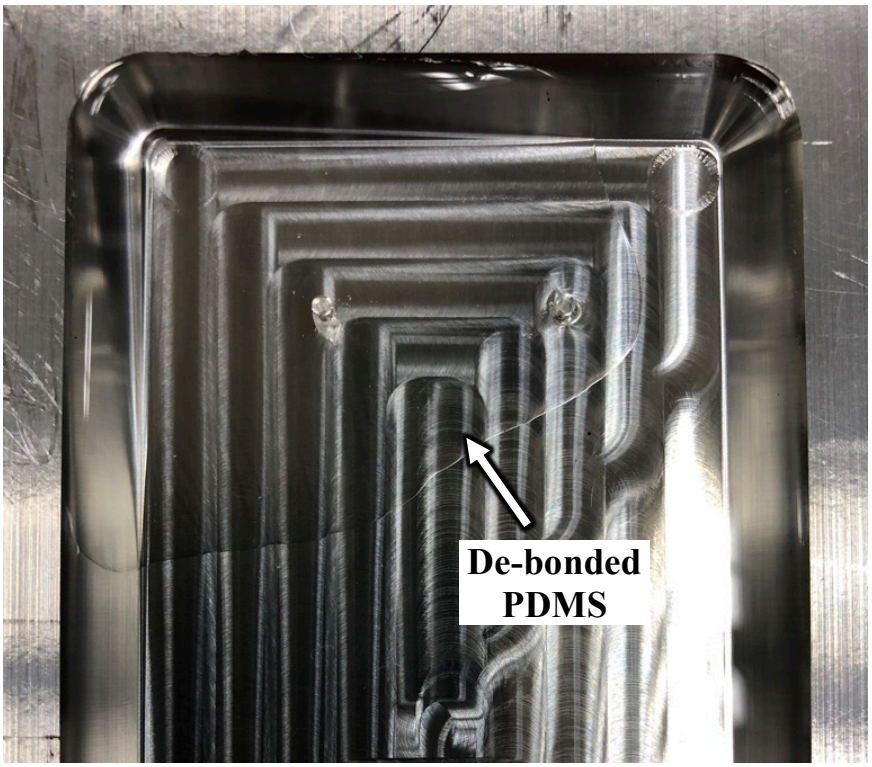

Figure 34 - Second needle location on the right de-bonded less PDMS after intersecting with the first de-bond on the left

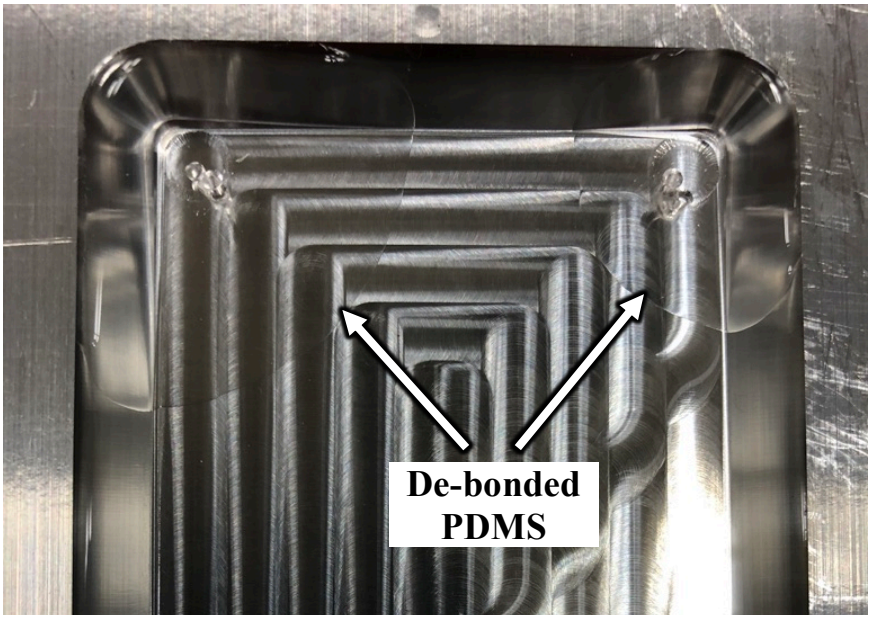

Figure 35 - Needle de-bond locations too far apart did not connect to each other

While greater distance inward can increase the de-bonded area, it must be reasonable for final automation, as the mold must be designed accordingly. This requires that the size of the bezel must be at least slightly larger than this distance inward, or the channels will leak through the hole created by the needle piercing.

This experiment resulted in two major findings regarding the wall type of the mold, and the use of two needle piercings. The two needle locations were intended to increase the width of the de-bond across the shorter edge (width) of the mold. However, it was found that a second needle de-bond will either connect to the previous site, leaving the surrounding walls still bonded (Figure 34), or de-bond to the wall, leaving the two areas unconnected (Figure 35).

5.2.4 *Retraction Speed and Location*

The previous experiment provided important findings regarding needle location, retraction speed, and chamfer vs. vertical wall molds. However, the peeling caused by the needle, as well as the use of two separate needle de-bonds, prevented the ability to obtain a precise relationship between the variables and their results. To obtain a more measurable comparison, a follow up test was performed.

The first tests were performed on 51 x 76 mm mold pockets, which is smaller than the current targeted mold dimensions of 127 x 127 mm. Although mold sizes will vary by the final application, testing larger molds can help isolate the variables by allowing the de-bond area to propagate further, without interacting with sidewalls. Therefore, the second experiment utilized a 127 mm square mold. Due to the chamfer wall mold exhibiting significantly less de-bond area, the next test only used a vertical wall mold to help better understand the variables. In the previous experiment, a retraction speed of 20 cm/s resulted

in unwanted peeling by the needle due to stronger adhesion at the slower retraction speed. For the next experiment, speeds of 30 and 60 cm/s were used, with a simple multiple to potentially assist in understanding the interactions. The needle locations are set at 5 and 10 mm inward from the edge, and positioned at mid-width of the edge. Figure 36 shows the testing plan.

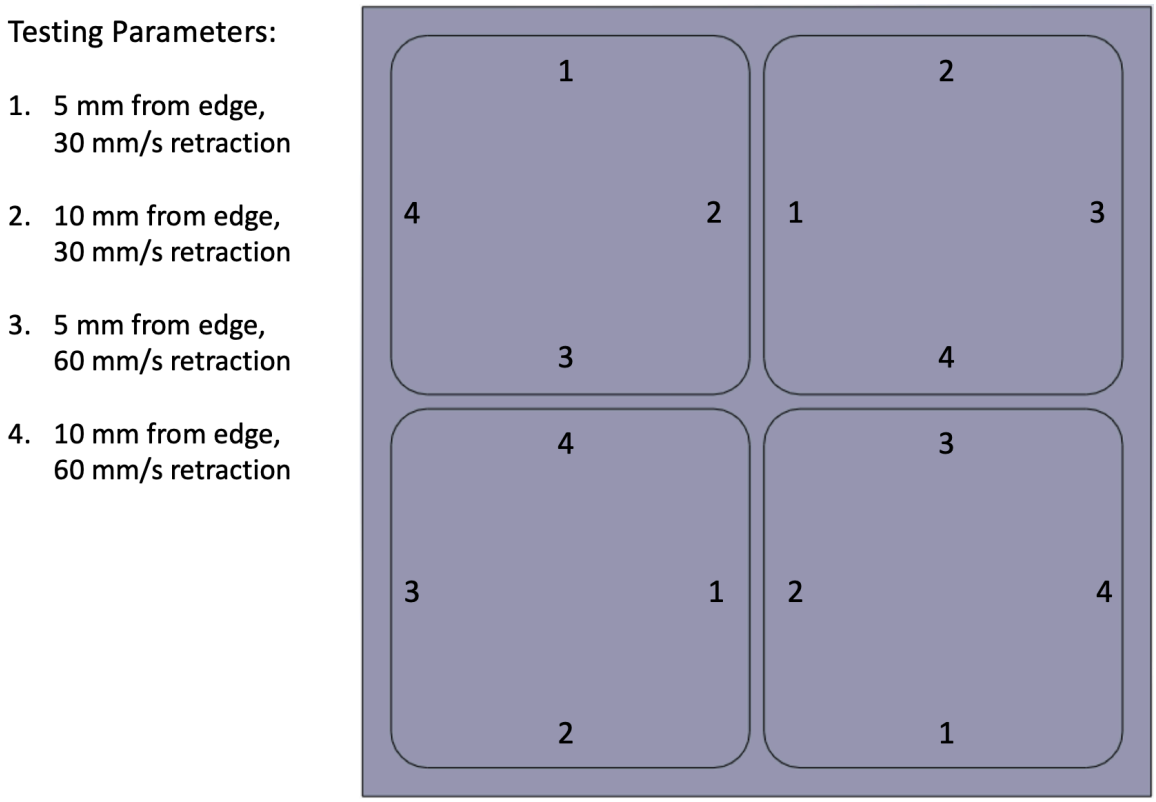

Figure 36 - Experimental plan for systematic testing the effects of needle location and retraction speed

Each of the four parameters are tested on each wall of the four pockets. This eliminates any bias caused by variations in the curing process, such as uneven temperature distribution caused by the oven or the aluminum mold.

5.2.5 *Results*

The test was performed twice, swapping test conditions on opposing edges of each pocket for the second test. For example, in Figure 36, the conditions for edges 1 and 3, and for edges 2 and 4 in the upper left pocket were swapped. This ensures complete uniformity of the testing parameters. Images were taken above the mold after each test, and the de-bond region traced in AutoCAD to measure the areas. Figure 37 and Figure 38 show the traced areas in each test of the two experiments, where Tests 1 through 4 are replications of each testing conditions indicated at the top of the column.

Figure 37 - First testing layout of retraction speed and needle placement

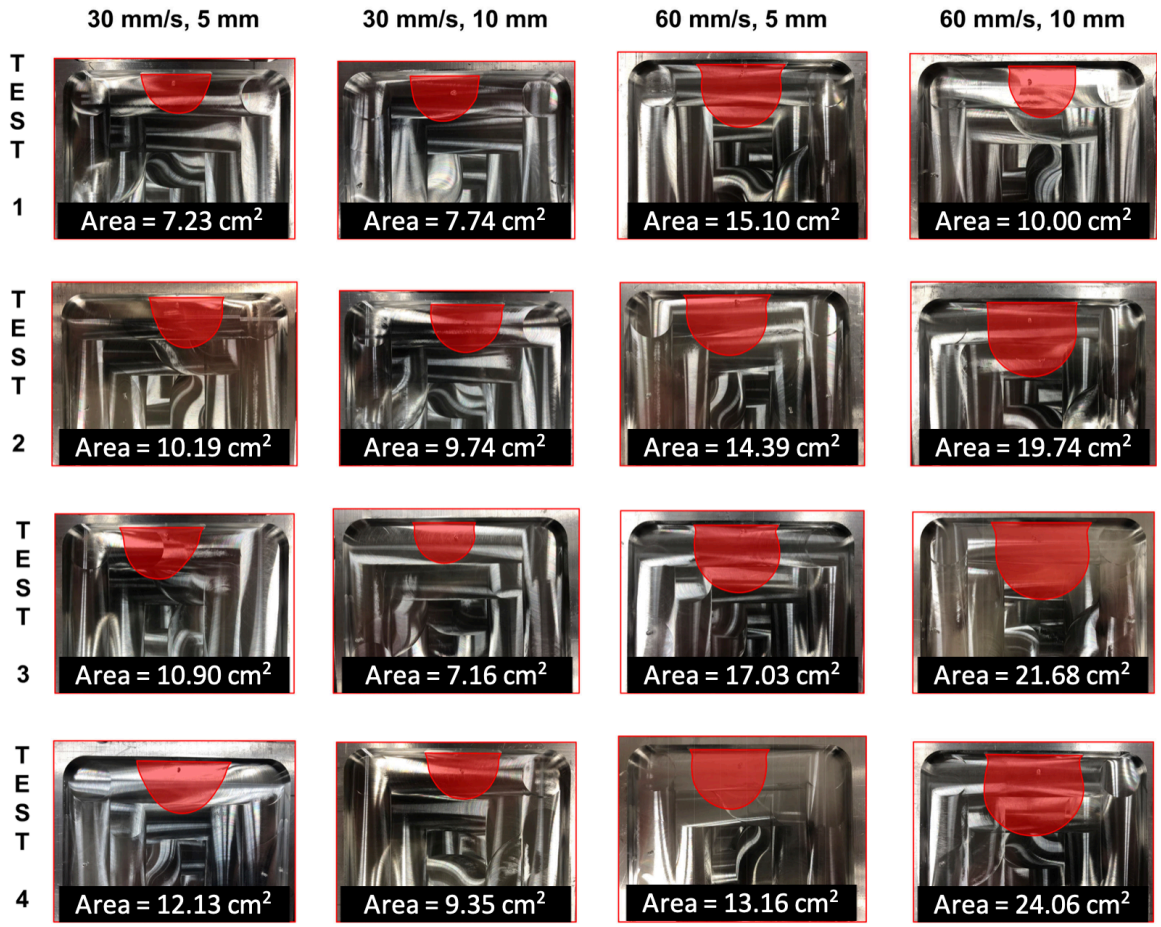

Figure 38 - Second testing layout of retraction speed and needle placement

The figures show that the two columns on the left of Figure 37 generally had considerably more de-bonded area than the columns on the right. This would support the idea that the slower retraction speed led to greater de-bonding. However, in Figure 38, when the test conditions were applied to the opposing edge, the opposite results occured, with more de-bonding on the right half. The cause of this was found during review of high speed video which showed that there was a slight needle angle generated during retraction, which caused the biased results above. This angle is due to a lack of rigidity in both the needle's LUER lock fitting, as well as in the robot joints. The slight needle angle causes the variation in de-bond area due to the initial direction of the air once the needle begins to

lift off the bottom of the mold. When the top of the needle is angled outward (away from the center of the mold pocket), the air is therefore directed toward the center of the mold, increasing the de-bond in this direction. Additionally, the needle angle presses down on the PDMS nearest to the wall, hindering the ability for the air pressure to escape. The opposite is true when the needle is angled inward toward the center of the mold pocket, causing air quickly to escape up the wall. Table 4 and Table 5 compare the de-bond areas of each experiment and the averages.

Table 4 - De-bond areas in the first testing layout of retraction speed and needle placement

	30 mm/s, 5 mm (cm^2)	**30 mm/s, 10 mm (cm^2)**	**60 mm/s, 5 mm (cm^2)**	**60 mm/s, 10 mm (cm^2)**
Test 1	20.65	7.81	6.58	8.65
Test 2	11.48	22.13	4.32	8.39
Test 3	16.19	17.68	10.06	6.77
Test 4	9.68	22.84	10.45	10.84
Average	14.50	17.61	7.85	8.66
Standard Deviation	4.93	6.93	2.93	1.67

Table 5 - De-bond areas in the second testing layout of retraction speed and needle placement

	30 mm/s, 5 mm (cm^2)	**30 mm/s, 10 mm (cm^2)**	**60 mm/s, 5 mm (cm^2)**	**60 mm/s, 10 mm (cm^2)**
Test 1	7.23	7.74	15.10	10.00
Test 2	10.19	9.74	14.39	19.74
Test 3	10.90	7.16	17.03	21.68
Test 4	12.13	9.35	13.16	24.06
Average	10.11	8.50	14.92	18.87
Standard Deviation	2.08	1.24	1.62	6.17

Table 6 - Averages and standard deviations of the first and second layouts

	30 mm/s, 5 mm (cm^2)	**30 mm/s, 10 mm (cm^2)**	**60 mm/s, 5 mm (cm^2)**	**60 mm/s, 10 mm (cm^2)**
Average	12.31	13.06	11.39	13.77
Standard Deviation	4.22	6.70	4.37	6.88
Advantaged Average	14.50	17.61	14.92	18.87
Disadvantaged Average	10.11	8.50	7.85	8.66

The overall averages in Table 6 show that the 10 mm needle location had a higher area de-bonded, however, the large standard deviation indicates that the needle angle is much more of a contributing factor. The comparison of the favorable versus unfavorable averages (needle angled outward vs. inward, respectively), shows that the slight needle angle can approximately double the area that is de-bonded. This experiment again shows that retraction speed has little impact on the de-bonding area.

The needle location and retraction speed has little effect on de-bonding area because the required air pressure to separate the sidewall of the mold, which allows the air to escape, is largely independent of either variable. The vertical walls of the mold, and the associated shear force of adhesion, has additional resistance to de-bonding when compared to continued propagation of the de-bond along the bottom surface of the mold. Therefore, the retraction speed, and more directly the location of the needle may only impact how quickly the air first reaches the wall. However, the additional resistance of the adhesion along the mold wall will nearly eliminate any differences between these variables.

5.2.6 *Angled Needle De-bonding*

The previous experiment showed that slight variations in needle angles can cause a significant impact on de-bonding area. While this variation can't be eliminated, it can be used advantageously. This finding inspired the intentional angling of the needle, rather than vertical retraction.

The next experiment was performed by first piercing the PDMS vertically as before. The needle was then raised a few millimeters upward off the bottom of the mold to remove the force from the needle (generated during piercing). The needle was then angled outward at varying degrees of 5, 10, and 20 degrees off vertical. Once the angle was reached, air pressure was activated. After de-bonding, the needle returned to vertical, and was retracted at 60 cm/s to prevent the needle from adhering to the PDMS. Intentionally angling the needle ensures that the needle is always facing in the desired direction, regardless of minor variations. Additionally, the exaggerated angle causes the needle to further press down on the top surface of the PDMS near the wall, greatly limiting the escape of air at the edge of the mold. Figure 39 is an image of the angled needle during de-bonding.

5.2.7 *Results*

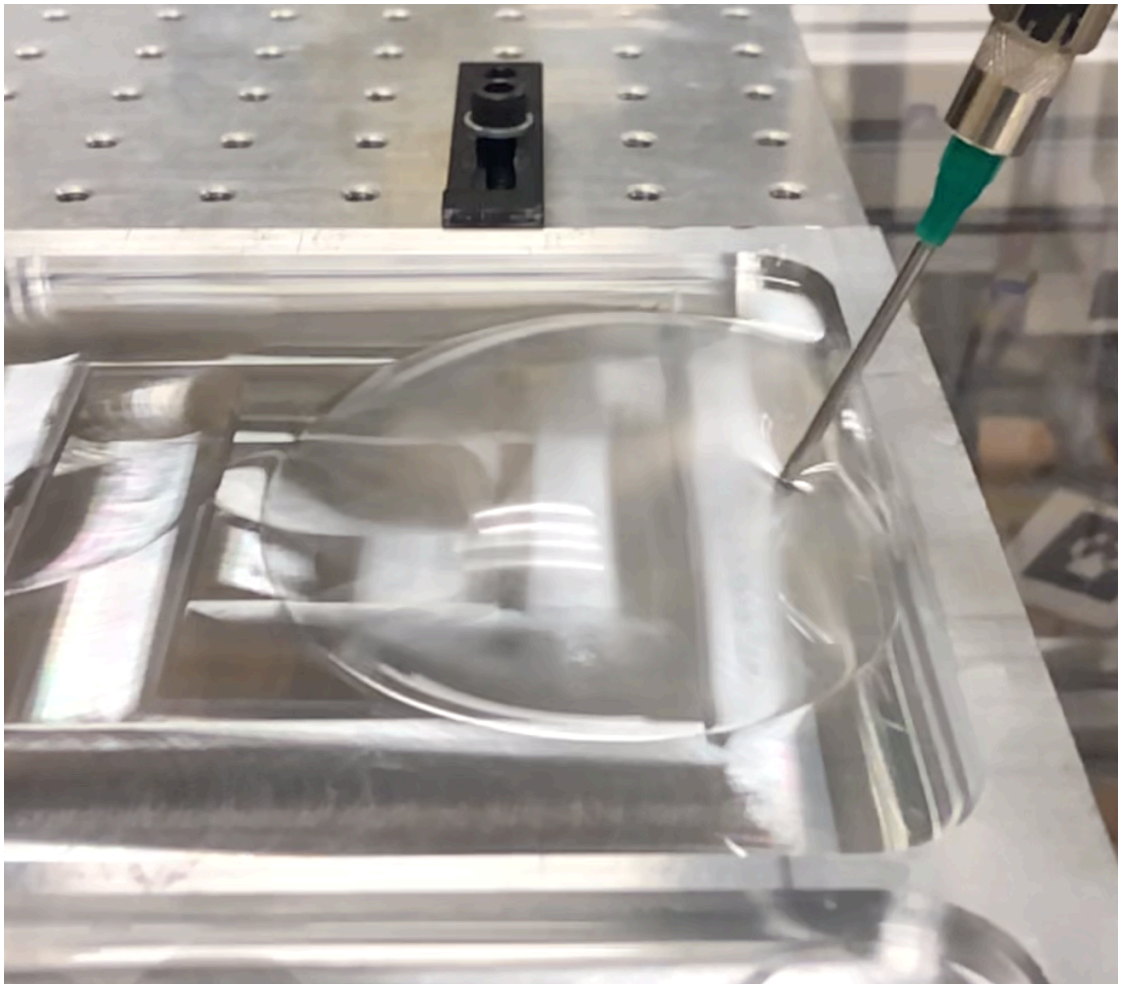

Figure 39 - Needle de-bonding at 20-degree angle. Image showing just prior to air escaping up the wall on the right

Figure 32 shows that the angled needle de-bonds the PDMS inward by an amount much greater than the distance of the needle from the wall, resulting in a large de-bond area. The areas de-bonded by needle angles 5, 10, and 20 degrees are compared in Figure 40.

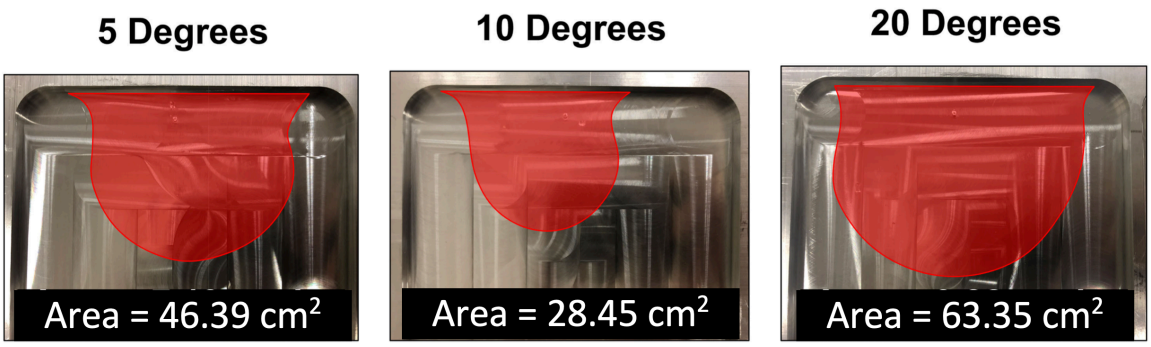

Figure 40 - Angled needle de-bond areas at 5, 10, and 20 degrees

Each angle de-bonded significantly more PDMS than the tests where the needle was vertical to the mold bottom, even those where the slight needle angle was in favor of increased de-bonding. However, given the reduced area of the 10-degree test, there isn't a reliable trend in observations. Instead, the area can vary by 100 percent or more as seen above, depending on which path the air naturally follows. The 10-degree test caused the de-bond to propagate mainly towards the left of the needle, until the air escaped.

5.2.8 *PDMS Anchoring Device*

The angled needle de-bonding experiment showed that directing the air, combined with anchoring the PDMS surface nearest to the wall, results in a considerable increase in de-bonded area. However, it was also observed in all experiments reported in this chapter, that there is an uncontrollable degree of randomness in the direction of de-bonding. This was shown above in the 10-degree needle angle, where the de-bond primarily traveled towards the left, rather than symmetrically. In the angled needle experiment, only the thin needle was acting to anchor the PDMS. Instead, a device can be incorporated to hold down the PDMS behind the needle. This anchor can be nearly the width of the mold pocket, to

ensure sufficient de-bonding inward. Figure 41 shows the needle attachment and PDMS anchoring robotic end-effector.

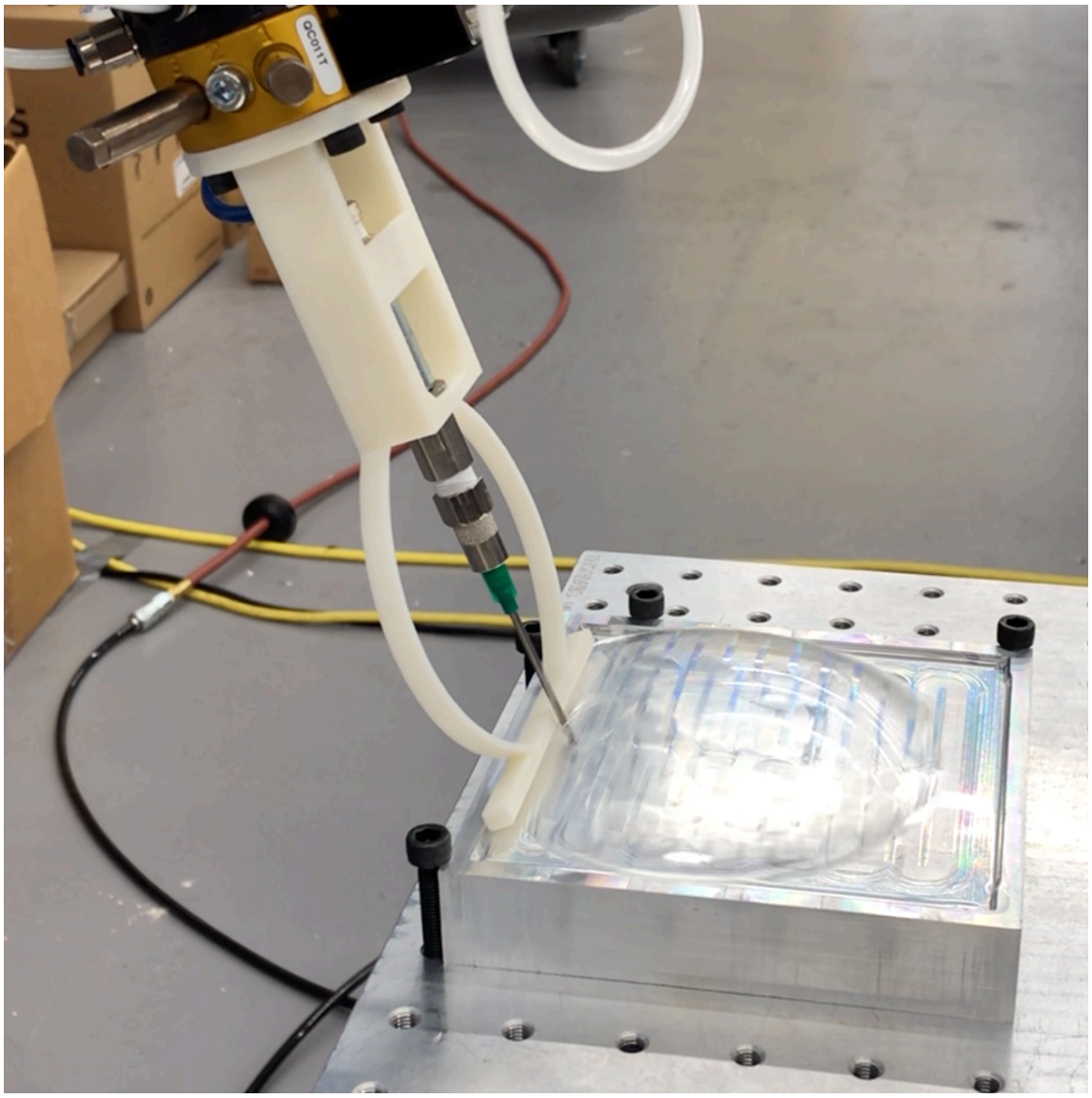

Figure 41 - De-bonding with PDMS anchoring needle attachment. Attachment arm holds down PDMS along back wall while air is directed inward toward center of mold (right of needle in picture)

The anchoring device is approximately flush with the bottom of the needle, or 1 mm shorter than the length of the needle as tested. This allows the anchoring device to come in contact with the PDMS as the needle pierces to the bottom of the mold. Prior to

angling the needle, the robot is once again lifted slightly to remove the force on the needle. As the needle tilts to initiate de-bonding, the anchoring device becomes compressed due to the shortened distance generated by the angle, as shown in Figure 42. The arc-shaped walls of the of the anchoring device all it to deflect under load, to apply an adequate amount of pressure to the PDMS to prevent air from escaping up the nearest back wall of the mold.

5.2.9 *Results*

The anchoring device, prevented flow up the wall nearest the needle, requiring the air to continue de-bonding until it reached one of the walls on either side of the needle. This led to de-bonds larger than any previous test, or consistently greater than 70 cm^2. De-bonded PDMS of this size is plenty large enough to enable suction peeling. However, the anchoring device prevents any de-bonding along the back wall. Given that this edge of the PDMS is first part to be lifted during peeling, suction peeling becomes unsuccessful. To solve this issue, the needle is angled the opposite direction of the initial de-bond while air pressure remains activated. This directs air toward the back wall, leading to complete de-bonding across the width of the mold.

While de-bonding was successful in some earlier experiments, particularly for the angled needle, the anchoring device ensures that the de-bond is consistently large enough to enable suction peeling.

5.2.10 *Needle De-bond Summary*

An understanding of needle piercing and de-bonding characteristics was acquired in this section. Larger diameter needles, such as 14-gauge, resulted in greater de-bonding,

while being more durable, reliable, and safe. Larger diameter needles allow for a higher air flow rate at the same pressure, increasing the rate of de-bonding prior to air escaping from underneath the PDMS. The PDMS required at least 35 N to pierce the PDMS, and about 30 N to continue penetrating the PDMS using a flat needle. The chamfered needle required slightly less force to pierce, however, the needle did not stop once contact with the mold was made, and instead continued to bend. This finding determined that a flat needle is most suitable for automation.

Experiments showed that needle placement and retraction speed alone did not provide reliable de-bonding. Instead, angling the needle directs the de-bonding inward, greatly increasing the area. To further maximize de-bonding area, a PDMS anchoring device was incorporated into the robot needle attachment. The anchoring device provided for consistently large de-bonded areas by preventing air from escaping up the mold wall nearest the needle.

5.3 Suction Peeling

Once de-bonding is complete, the PDMS can be peeled and removed using suction cups. Suction cups are ideal for automation due to their versatility in peeling any sized mold, without requiring custom devices. Suction cups can lift or release PDMS simply by activating the air pressure. The suction cup can then be used on the next device. In contrast, mechanical devices used to peel PDMS will likely contain residue, which would need cleaning between operations.

5.3.1 *Design*

For a suction cup to generate a suction force, a vacuum pump was used. The vacuum pump used in this work was a Piab VGS2010. The VGS2010 can accept a variety of suction cup shapes and sizes, however, a 25 mm diameter suction cup is adequate for testing a variety of mold sizes. The UR5 robot was equipped with pressurized air tubes for operating the end effector. A pressure of 60 psi was used for suction peeling as well. As with the robotic needle attachment, the suction cup was mounted to the robot using a 3D printed bracket. The air pressure of the robot travels through the tool plate, which allows for end effectors to be interchanged automatically. Figure 42 shows the suction cup attachment.

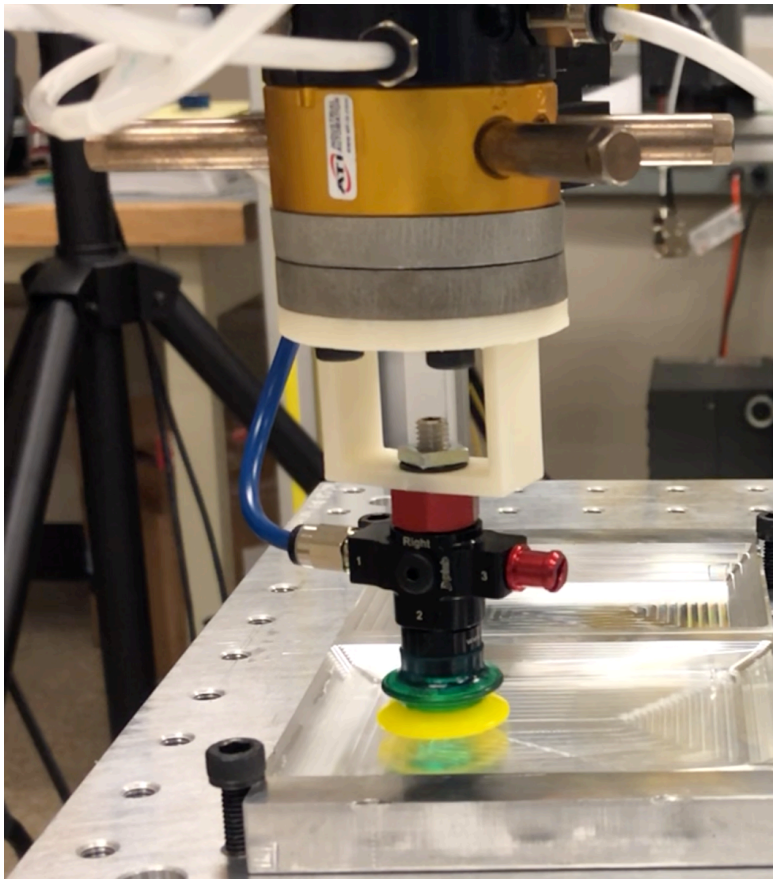

Figure 42 - Suction cup robotic end-effector

5.3.2 *Suction Properties*

Prior to automated testing of suction cup-based peeling and removal of PDMS, an understanding of the basic characteristics must be obtained. In order to peel the PDMS with a suction cup, the suction must be great enough to withstand the approximately 7 N generated in earlier tests, although this value will vary by mold. To test the maximum suction force, the robot lowered the suction cup to make complete contact with a bonded section of PDMS. Bonded PDMS was used to ensure that the grip of the suction cup will fail without the PDMS lifting. Air was then activated, and the robot was raised upward (normal to the surface of the mold) at 1 mm/s. The ATI sensor recorded 18 N of force, proving that the suction cup is capable of peeling PDMS if the peeling process was preceded by suitable de-bonding of the PDMS. After it was determined that the suction cup can peel the PDMS, the ideal placement of the suction cup on the PDMS and its motion must be determined. This is best done by operating the suction cup by hand, without it being attached to the robot.

The objective of the de-bonding process was to overcome the adhesion between the PDMS and the metal mold over as great an area as possible, to assist in peeling. However, the minimum extent of de-bonding to allow peeling must be determined. The suction cup was positioned with an increasing overlap over a de-bonded area of PDMS. After several tests, it was found that at least 50 percent of the suction cup must overlap the de-bonded PDMS, or the adhesive forces are greater than the suction forces. With an overlap of slightly less than 50 percent, the PDMS cannot be peeled. However, with over 50 percent overlap, the PDMS peels easily with little resistance, regardless of the peeling path of the suction cup. In order for the peel to travel the length of the mold pocket, the PDMS must

be continuously lifted upward, which causes the de-bonded section to propagate across the PDMS layer. When less than 50 percent of the suction cup overlaps the de-bonded PDMS, the pulling force is normal to a majority of the PDMS, preventing the initial lift of the leading edge. Instead, with more than 50 percent coverage, the upward pulling force quickly angles the PDMS, allowing for propagation of the de-bond.

Another critical aspect of suction cup placement is ensuring that it is not positioned over the hole in the PDMS created by insertion of the air needle. The hole allows the vacuum pressure to travel through, which creates a suction force between the PDMS and mold, preventing lifting. Alternatively, if the PDMS does occasionally initiate the peel with the suction cup over the hole created by needle piercing, the suction pressure will be lost and the PDMS will fall back down. This is the reason why successful de-bonding of a large area is critical.

Manual peel testing found that the suction cup can successfully peel in a variety of paths. However, the most natural technique involves rotating the suction cup while lifting upward slightly, similar to turning a page in a book. Once the suction cup is rotated to about 45 degrees, traveling on a 45-degree path results in a successful peel without unwanted stresses on the PDMS.

5.3.3 *Peeling*

The suction cup based peeling process was automated using the robot teach pendant. The suction cup was first lowered to make complete contact with a de-bonded section of PDMS. The air pressure was then activated. The robot was then simultaneously lifted upward and toward its base by about 10mm, while rotating to a 45-degree angle. This lifts the PDMS layer's leading edge, which requires nearly zero force due to the minimal

adhesion present after de-bonding. Once the leading edge is lifted, peeling of the bonded portion of the PDMS can proceed. This is performed by peeling along a straight 45-degree path upward over the mold. Figure 43 through Figure 45 show the three steps of peeling including the initial contact, rotation, and peeling.

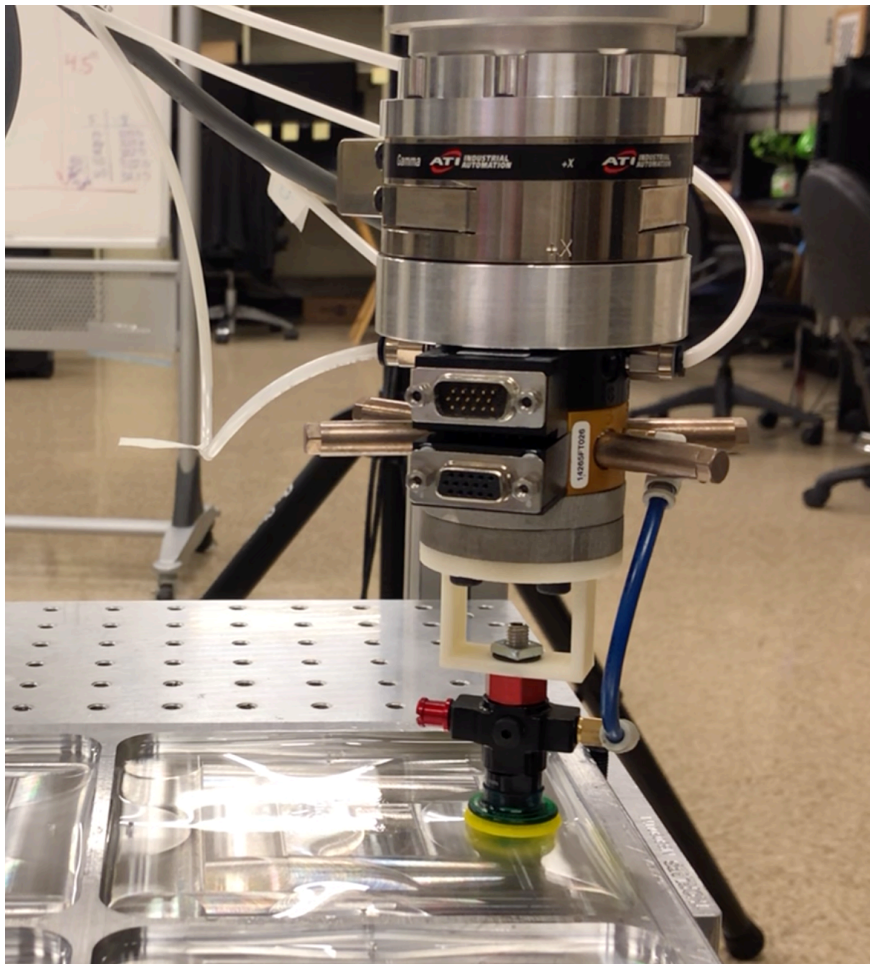

Figure 43 - First step of suction peeling. Robot lowers suction cup to PDMS and activates air pressure to generate vacuum

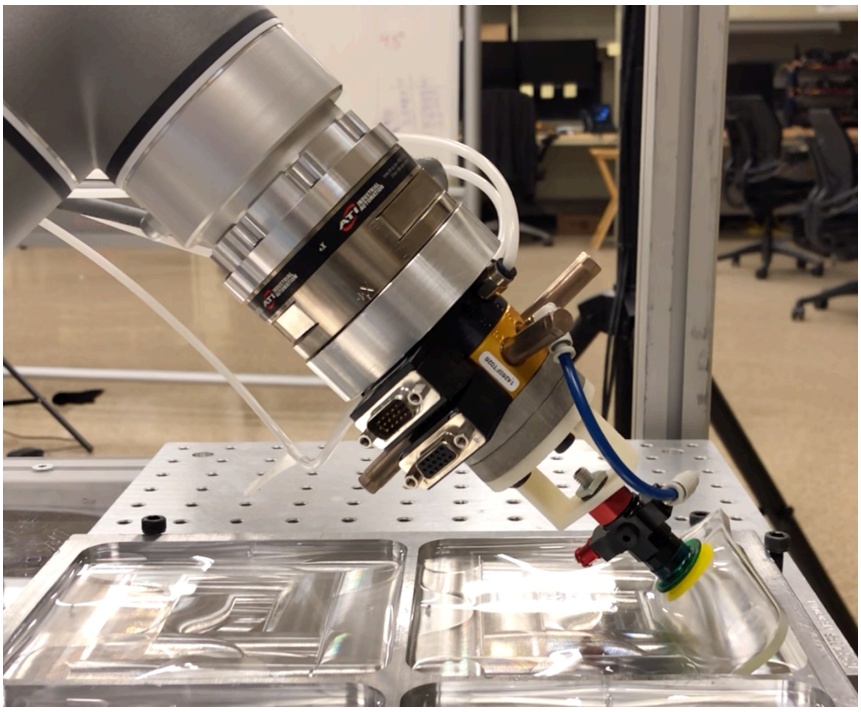

Figure 44 - Second step of suction peeling. Robot rotates to 45 degrees while lifting upward slightly to initiate peeling

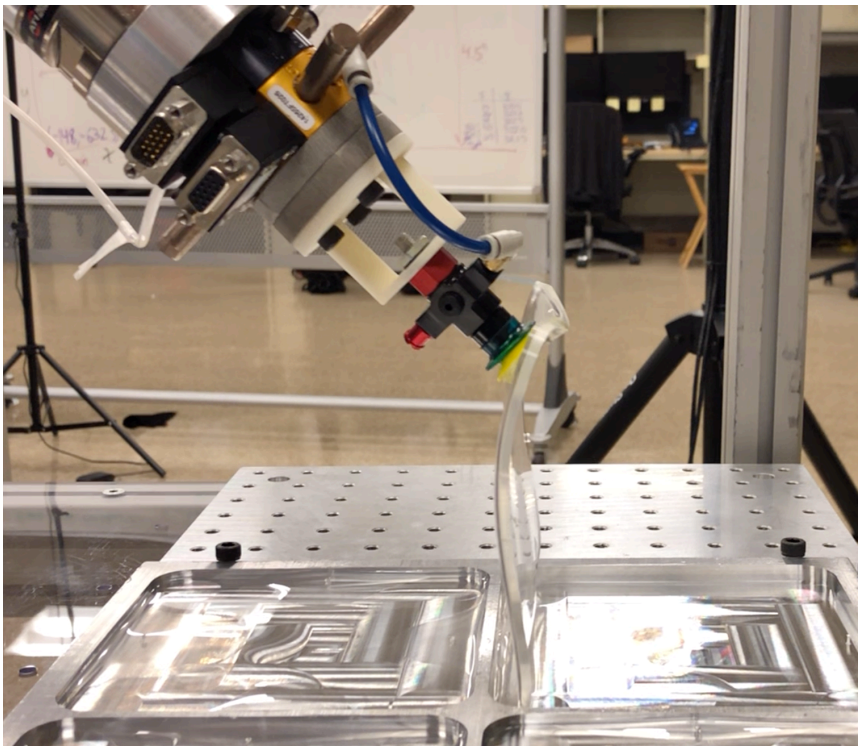

Figure 45 - Third and final step of suction peel. Robot travels in a straight line along a 45-degree path to remove PDMS from the mold

Figure 45 shows the bottom half of the suction cup at a steep angle relative to the PDMS. This is undesirable as it can lead to the suction cup separating from the PDMS, causing a failed peel. To address this concern, the suction cup continues tilting during the peel path. Therefore, after the initial tilt of 45-degrees, the suction cup continues tilting an additional 15 degrees throughout the peel path, finishing at a 60-degree angle (from vertical). This better aligns the suction cup and PDMS to mitigate separation of the suction cup from the PDMS during peeling.

5.3.4 *Results*

Using this peeling method, there were both successful and unsuccessful peeling attempts. The unsuccessful peels occurred when smaller areas were de-bonded, which required the suction cup to first peel the PDMS layer outward along the width of the mold pocket, before continuing to peel along the length of the mold in the direction of the peel path. This additional stress on the suction cup caused it to separate from the PDMS. This was addressed by incorporating the PDMS anchoring device to ensure a larger de-bonded area before air escaped from under the PDMS. Additionally, on wider PDMS layers, multiple suction cups across the width of the PDMS could be used simultaneously on the same robot attachment to distribute the load.

After the PDMS layer is peeled, it must be transported to an area for stacking and assembly into the multi-layer PDMS based microfluidic device. With one or multiple suction cups located only along the leading edge, the PDMS will bend downward due to gravity. This prevents the robot from placing the PDMS straight down onto a horizontal surface. Additional suction cups can be used on the other half of the PDMS layer to control the flexible device. This would require that the suction cups to either be located on the

same robot attachment, or a second robot to perform the stacking process. Alternatively, the robot could be rotated as the PDMS is placed in the desired location, similar to a reverse peeling motion. While it would require a more advanced automation procedure, it would eliminate the need for an additional robot or a more complex custom robot attachment.

5.3.5 *Suction Peeling Summary*

The process of suction peeling is much more forgiving than the de-bonding step. As discussed earlier, de-bonding required precise steps to overcome the adhesive forces. In contrast, when successful de-bonding precedes the PDMS removal process, suction cup-based peeling can be successful without requiring exact steps to be followed. However, the process can be optimized by peeling along a path that keeps the surface of the suction cup parallel to the surface of the PDMS. This ensures that there is equal force around the diameter of the suction cup, maximizing the lifting capacity and increasing the reliability for final automation.

The results in this chapter showed that the edge of the PDMS that was de-bonded could be lifted with ease, and could be rotated to prepare for the continuous peel across the entire length of the mold. Lastly, it was shown that the PDMS can be placed for stacking and assembly of the microfluidic device by reversing the peeling motion in order to lay the device down flat.

CHAPTER 6. CONCLUSION

This thesis discussed the challenges of microfluidic device production using existing (largely manual) methods, and proposed and investigated alternate methods and equipment for flexible automation using a 6-dof articulated arm robot. The manual methods currently used in photolithography-based microfluidic device production are impractical for automated production of microfluidic devices. To date, automation has not been achieved due to the innovation required to replace the manual steps, via a repeatable robotic process.

To first prepare the production process for automation, a more durable approach to molding must be used. Photolithography on silicon wafers is expensive, time consuming, and has a short lifespan. Machined metal molds have become more common, as they can be reused to produce the PDMS device layers. While there are guidelines for machining metals using the milling process, adequate machining procedures for producing a microfluidic device metal mold are lacking. This required experimentation to find suitable machining parameters. The standard recommended milling feeds and speeds for traditional cutting do not provide an adequate surface finish for use in microfluidic mold making. Instead, a slow feed rate of 5 in/min should be used, as it minimizes the feed per tooth, improving the surface finish of the mold. Additionally, the slower feed rate essentially eliminates tool deflection, further improving surface flatness. This feed rate, however, still allows for a for a reasonable machining time of approximately 30 minutes to an hour, depending on the mold dimensions. Higher spindle speeds also reduce the feed per tooth, lowering surface roughness. The Okuma CNC milling machine that was used for this work

had a maximum spindle speed of 12,000 rpm, although higher speeds could be beneficial. Achieving the smoothest surface with precise tolerancing is desirable, however, an exact baseline for these parameters have not yet been determined by the scientific community.

Most of the steps involved in PDMS preparation and curing involve simple tasks that are amenable to automation. However, automating the removal of the cured PDMS layer from the metal mold requires new methods and equipment have not been previously explored. This requires a deeper understanding of the PDMS as it is removed from the mold, followed by an investigation of methods to automate the peeling process.

Given the targeted market for the final microfluidic device production process, all equipment should be low cost, and, where possible, utilize readily available equipment. Initial attempted methods of peeling involved mechanical devices including embedded tabs and grippers. It was found that physical devices exert pressure on a large enough surface area to generate considerable adhesive forces. These forces prevent the PDMS layer from being separated from the mold. Attempts to minimize the contact area with the PDMS, such as with a bladed gripper, requires a level of precision that is unsuitable for robotic automation.

In order to prepare the PDMS for peeling, it must first be de-bonded to reduce the adhesive forces. Since it was found that mechanical devices are unable to reliably overcome the initial adhesion between the PDMS and the aluminum mold, air pressure was used instead. This thesis shows that by introducing pressurized air between the PDMS and mold, de-bonding can be achieved. The most practical method of introducing air is by completely piercing the PDMS with a dispensing needle through to the bottom surface of the mold. While de-bonding can occur by simply blowing air during needle retraction, a

more effective method incorporates an anchoring device to better direct the air to a large portion of the bonded PDMS to maximize the de-bonded area.

Following a successful de-bonding process, the PDMS can be peeled using a suction cup. Suction cups have no moving parts and can be used reliably and repeatedly. Additionally, suction cups do not damage the PDMS device, which could occur with other methods such as bladed grippers. In order to initiate a successful peeling process, the suction cup must be positioned so that at least 50 percent of the suction cup overlaps the de-bonded PDMS, without being placed over the hole from the needle pierce, or vacuum loss will occur. On wider molds, such as a 127 mm mold, the use of more than one suction cup can better distribute the load, increasing the reliability of the peel. After peeling, the suction cup can transport the PDMS to the final stacking location, utilizing a reverse peeling technique to lay the peeled PDMS down.

This thesis has paved a path forward to final automation of microfluidic device production. Based on the literature search conducted for this thesis, previously, there are no known methods of completely automating the device production process. The innovative use of automated de-bonding and peeling techniques investigated in this thesis provide strong guidance for further development of automated microfluidic device production. The techniques presented can be refined for optimal results, which will involve additional experiments.

CHAPTER 7. FUTURE DEVELOPMENTS

The overall objective of this research was to understand the exact methods required to replace the manual approach of microfluidic device production with a set of processes capable of robotic automation. There has been success in developing these methods, however, the robotic operations must now be optimized. The experimentation in this thesis was performed by programing the robotic with exact coordinates, which is not a reliable technique for final automation. More generally, automation for all steps in the production process must be created. This involves everything from PDMS mixing and pouring, through to final assembly bonding.

7.1 Preparing PDMS and Molding

This thesis focused on the PDMS removal process, as it was the most technologically challenging step in the automation. However, for complete automation prepared for the end user, all steps must be programed and refined. Many of these steps are simple tasks for the robot but will involve additional equipment to carry out. First, the raw materials of the PDMS must be in a known location for the robot to lift and pour with a gripper. The ATI force sensor can be utilized to measure the proper amount of polymer and crosslinker. An end effector with a mixing attachment can then mix the PDMS. The PDMS container must then be placed in a vacuum desiccator with the gripper attachment, to remove air bubbles. After a set period of time, the PDMS is then ready to be poured in the mold, and then the mold transported to an oven for curing. To prepare the mold for de-bonding and peeling, it must be secure to a table. Spring loaded fasteners may be useful in

quickly and easily positioning the mold. The PDMS is then ready for the de-bonding and peeling steps.

7.2 Fully Automated De-bonding, Peeling, and Assembly

As discussed, the automation used during experimentation used the included teach pendant for coding exact coordinates. However, hard-coding points into the robot will not allow for versatile operation of various mold sizes. Instead, a program should be created to initialize the parameters at the start of the automation process. Zeroing the mold dimensions can be performed by positioning the robot end effector off to the side of a secured mold. With the height of the end effector below the top of the mold, it will travel toward the mold until a force is detected. This method can be used to determine the X and Y origin, as well as the length and width of the mold. With these dimensions, the robot can then be raised above the top of the mold and positioned near a corner or edge. The robot will then be lowered to determine the height of the mold, useful for finding the clearance.

Following the recording of origin and dimensions, de-bonding can proceed. Rather than programing a certain extent of "overlap" between the needle and the mold to generate the desired force, an optimized velocity-stop program can ensure that the exact desired piercing force is met. With the length and width of the mold pocket known, a corresponding peel and placement path can be generated. This is particularly associated with the length of the mold, as it involves how much the suction cup should rotate per unit length of the PDMS. This ensures that an ideal contact angle between the PDMS and suction cup is maintained.

Lastly, after the PDMS is placed down on a substrate, the bonding process must be programed. The most affordable method of bonding PDMS to glass or PDMS is using a

corona wand treatment. Corona treatment discharges plasma which bonds the molecules between the layers, securely enclosing the channels of the microfluidic device. Corona wands are handheld devices which can be gripped with the robot. The wand can then be passed above the surface in an optimized fashion to complete the microfluidic device production.

7.3 User Interface

All of the tasks discussed in this chapter require the efforts of computer scientists to generate and refine the robotic programing. However, the end user will have expertise in the areas of biology and chemistry, rather than in computer coding. For automation to be suitable for these industries, a simple user interface (UI) must be created. The UI should involve simple start and pause options, as well as the ability to begin or repeat certain steps.

Automation of microfluidic device production is a valuable advancement in engineering. The completion of the contributions of this thesis will allow for reduced production costs and labor, and promote increased bio-chemical research.

REFERENCES

[1] R. Tran et al., "Microfluidic Transduction Harnesses Mass Transport Principles to Enhance Gene Transfer Efficiency," Molecular Therapy, vol. 25, no. 10, pp. 2372–2382, Oct. 2017.

[2] C. Iliescu, H. Taylor, M. Avram, J. Miao, and S. Franssila, "A practical guide for the fabrication of microfluidic devices using glass and silicon," Biomicrofluidics, vol. 6, no. 1, p. 16505, Mar. 2012.

[3] H. Becker, "Polymer microfluidic devices," Talanta, vol. 56, no. 2, pp. 267–287, 2002.

[4] "PDMS: A review," Elveflow. [Online]. Available: https://www.elveflow.com/microfluidic-tutorials/microfluidic-reviews-and-tutorials/the-poly-di-methyl-siloxane-pdms-and-microfluidics/.

[5] S. Ng, R. Tjeung, and Z. Wang, "Hot embossing on polymethyl methacrylate," in 2006 8th Electronics Packaging Technology Conference, 2006.

[6] T. D. Boone, Z. H. Fan, H. H. Hooper, A. J. Ricco, H. Tan, and S. J. Williams, "Peer Reviewed: Plastic Advances Microfluidic Devices," Analytical Chemistry, vol. 74, no. 3, p. 78 A-86 A, Feb. 2002.

[7] J. W. Park, B. Vahidi, A. M. Taylor, S. W. Rhee, and N. L. Jeon, "Microfluidic culture platform for neuroscience research," Nature Protocols, vol. 1, no. 4, pp. 2128–2136, Nov. 2006.

[8] A. M. Christensen, D. A. Chang-Yen, and B. K. Gale, "Characterization of interconnects used in PDMS microfluidic systems," Journal of Micromechanics and Microengineering, vol. 15, no. 5, pp. 928–934, Mar. 2005.

[9] D. Fuard, T. Tzvetkova-Chevolleau, S. Decossas, P. Tracqui, and P. Schiavone, "Optimization of poly-di-methyl-siloxane (PDMS) substrates for studying cellular adhesion and motility," Microelectronic Engineering, vol. 85, no. 5–6, pp. 1289–1293, May 2008.

[10] J. Wang, M. Zheng, W. Wang, and Z. Li, "Optimal protocol for moulding PDMS with a PDMS master," Chips and Tips. [Online]. Available: http://blogs.rsc.org/chipsandtips/2010/07/06/optimal-protocol-for-moulding-pdms-with-a-pdms-master/?doing_wp_cron=1560455252.7644240856170654296875.

[11] Z. Zhou, D. Chen, X. Wang, and J. Jiang, “Milling Positive Master for Polydimethylsiloxane Microfluidic Devices: The Microfabrication and Roughness Issues,” Micromachines, vol. 8, no. 10, p. 287, Sep. 2017.

[12] C. Yousuff, M. Danish, E. Ho, I. Kamal Basha, and N. Hamid, “Study on the Optimum Cutting Parameters of an Aluminum Mold for Effective Bonding Strength of a PDMS Microfluidic Device,” Micromachines, vol. 8, no. 8, p. 258, Aug. 2017.

[13] J. S. Mecomber, D. Hurd, and P. A. Limbach, “Enhanced machining of micron-scale features in microchip molding masters by CNC milling,” International Journal of Machine Tools and Manufacture, vol. 45, no. 12–13, pp. 1542–1550, Oct. 2005.

[14] I. R. G. Ogilvie, V. J. Sieben, C. F. A. Floquet, R. Zmijan, M. C. Mowlem, and H. Morgan, “Reduction of surface roughness for optical quality microfluidic devices in PMMA and COC,” Journal of Micromechanics and Microengineering, vol. 20, no. 6, p. 65016, May 2010.

[15] M. L. Hupert et al., “Evaluation of micromilled metal mold masters for the replication of microchip electrophoresis devices,” Microfluidics and Nanofluidics, vol. 3, no. 1, pp. 1–11, Jun. 2006.

[16] “Speeds & Feeds,” Niagara Cutter. [Online]. Available: https://www.niagaracutter.com/speedfeed.

[17] “Roughness of Si Wafer,” MikroMasch. [Online]. Available: https://www.spmtips.com/how-to-choose-afm-probes-by-applications-metrology-roughness-of-Si-wafer.html.

[18] D. Armani, C. Liu, and N. Aluru, “Re-configurable fluid circuits by PDMS elastomer micromachining,” Technical Digest. IEEE International MEMS 99 Conference. Twelfth IEEE International Conference on Micro Electro Mechanical Systems (Cat. No.99CH36291), pp. 222–227, 1999.

[19] S. Kim et al., “Microstructured elastomeric surfaces with reversible adhesion and examples of their use in deterministic assembly by transfer printing,” Proceedings of the National Academy of Sciences, vol. 107, no. 40, pp. 17095–17100, Sep. 2010.

[20] M. A. Meitl et al., “Transfer printing by kinetic control of adhesion to an elastomeric stamp,” Nature Materials, vol. 5, no. 1, pp. 33–38, Dec. 2005.

[21] I. Byun, A. W. Coleman, and B. Kim, “Transfer of thin Au films to polydimethylsiloxane (PDMS) with reliable bonding using (3-mercaptopropyl)trimethoxysilane (MPTMS) as a molecular adhesive,” Journal of Micromechanics and Microengineering, vol. 23, no. 8, p. 85016, Jul. 2013.

[22] K. Kendall, “Thin-film peeling-the elastic term,” Journal of Physics D: Applied Physics, vol. 8, no. 13, pp. 1449–1452, 1975.

[23] Y. Yu, D. Sanchez, and N. Lu, “Work of adhesion/separation between soft elastomers of different mixing ratios,” Journal of Materials Research, vol. 30, no. 18, pp. 2702–2712, Aug. 2015.

[24] D. Baek, S. Saito, and K. Takahashi, “Estimating work of adhesion using spherical contact between a glass lens and a PDMS block,” Journal of Adhesion Science and Technology, vol. 32, no. 2, pp. 158–172, Jun. 2017.

[25] R. W. R. L. Gajasinghe et al., “Experimental study of PDMS bonding to various substrates for monolithic microfluidic applications,” Journal of Micromechanics and Microengineering, vol. 24, no. 7, p. 75010, Jun. 2014.

[26] A. San-Miguel and H. Lu, “Microfluidics as a tool for C. elegans research,” WormBook, pp. 1–19, Sep. 2013.

[27] M. A. Eddings, M. A. Johnson, and B. K. Gale, “Determining the optimal PDMS–PDMS bonding technique for microfluidic devices,” Journal of Micromechanics and Microengineering, vol. 18, no. 6, p. 67001, Apr. 2008.

[28] S. Bhattacharya, A. Datta, J. M. Berg, and S. Gangopadhyay, “Studies on surface wettability of poly(dimethyl) siloxane (PDMS) and glass under oxygen-plasma treatment and correlation with bond strength,” Journal of Microelectromechanical Systems, vol. 14, no. 3, pp. 590–597, Jun. 2005.

[29] Y. Li, D. Sameoto, and C. Menon, “Enhanced compliant adhesive design and fabrication with dual-level hierarchical structure,” Journal of Bionic Engineering, vol. 7, no. 3, pp. 228–234, Sep. 2010.

[30] R. Dahiya, G. Gottardi, and N. Laidani, “PDMS residues-free micro/macrostructures on flexible substrates,” Microelectronic Engineering, vol. 136, pp. 57–62, Mar. 2015.

[31] J. Rajagopalan and M. T. A. Saif, “Fabrication of Freestanding 1-D PDMS Microstructures Using Capillary Micromolding,” Journal of Microelectromechanical Systems, vol. 22, no. 5, pp. 992–994, Oct. 2013.

[32] J. Zhou, A. V. Ellis, and N. H. Voelcker, “Recent developments in PDMS surface modification for microfluidic devices,” ELECTROPHORESIS, vol. 31, no. 1, pp. 2–16, Jan. 2010.

[33] PDMS. [Online]. Available: http://www.mit.edu/~6.777/matprops/pdms.htm.

[34] K. Haubert, T. Drier, and D. Beebe, “PDMS bonding by means of a portable, low-cost corona system,” Lab on a Chip, vol. 6, no. 12, p. 1548, 2006.

[35] C. Yang, W. Wang, and Z. Li, “Optimization of corona-triggered PDMS-PDMS bonding method,” in 2009 4th IEEE International Conference on Nano/Micro Engineered and Molecular Systems, 2009.

[36] P. E. Mallon, T. H. Berhane, C. J. Greyling, W. L. Vosloo, H. Chen, and Y. C. Jean, “Corona Treated Polydimethylsiloxane (PDMS) Surfaces Studied by the Slow Positron Beam Technique,” Materials Science Forum, vol. 445–446, pp. 322–324, Jan. 2004.